

Received March 31, 2020, accepted April 9, 2020, date of publication April 14, 2020, date of current version April 30, 2020.

Digital Object Identifier 10.1109/ACCESS.2020.2987873

Hardware- and Interference-Limited Cognitive IoT Relaying NOMA Networks With Imperfect SIC Over Generalized Non-Homogeneous Fading Channels

SULTANGALI ARZYKULOV¹, (Member, IEEE),
GALYMZHAN NAURYZBAYEV¹, (Member, IEEE),
MOHAMMAD S. HASHMI¹, (Senior Member, IEEE),
AHMED M. ELTAWIL², (Senior Member, IEEE),
KHALED M. RABIE³, (Member, IEEE), AND SHAKHMARAN SEILOV⁴

¹School of Engineering and Digital Sciences, Nazarbayev University, 010000 Nur-Sultan, Kazakhstan

²Computer, Electrical and Mathematical Science and Engineering Division, King Abdullah University of Science and Technology, Thuwal 23955, Saudi Arabia

³Department of Engineering, Manchester Metropolitan University, Manchester M15 6BH, U.K.

⁴Faculty of Information Technologies, L.N. Gumilyov Eurasian National University, 010000 Nur-Sultan, Kazakhstan

Corresponding author: Sultangali Arzykulov (sultangali.arzykulov@nu.edu.kz)

This work was supported in part by the Nazarbayev University Faculty Development Competitive Research Program under Grant 240919FD3935.

ABSTRACT Internet-of-Things (IoT) technology has received much attention due to its great potential to interconnect billions of devices in a broad range of applications. IoT networks can provide high-quality services for a large number of users and smart objects. On the other hand, massive connectivity in IoT networks brings problems associated with spectral congestion. This issue can be solved by applying cognitive radio (CR) and non-orthogonal multiple access (NOMA) techniques. In this respect, this paper studies the performance of cooperative CR-NOMA enabled IoT networks over a generalized $\alpha - \mu$ fading channel model. Closed-form analytical expressions of the end-to-end outage probability (OP) for the secondary NOMA users are derived using the Meijer's G-function with a consideration of the impacts of the interference temperature constraint, primary interference, residual hardware impairments and imperfect successive interference cancellation. Moreover, to acquire some useful insights on the system performance, asymptotic closed-form OP expressions are provided. Additionally, the impact of α and μ fading parameters on the outage performance is examined and, as a result, it is concluded that the system performance sufficiently improves as α and/or μ increase. Furthermore, the outage performance of the proposed system model is shown to outperform that of an identical IoT network operating on orthogonal multiple access. Finally, the provided closed-form OP expressions are validated with Monte Carlo simulations.

INDEX TERMS $\alpha - \mu$ fading, cognitive radio (CR), cooperative communications, Internet-of-Things (IoT), non-homogeneous generalized fading, non-orthogonal multiple access (NOMA), outage probability (OP).

I. INTRODUCTION

The Internet-of-Things (IoT) paradigm has recently received much attention, with research covering technology advances in several emerging wireless applications, such as device-to-device (D2D) [1], body area networks [2] and vehicle-to-vehicle [3] communications. By taking advantage of proximity, reuse, and hop gains of D2D communications [4],

The associate editor coordinating the review of this manuscript and approving it for publication was Mauro Fadda¹.

IoT networks can deliver a superior performance in terms of energy consumption, spectral efficiency, and low latency [5]. On the other hand, due to the massive connectivity and high traffic volume, IoT networks demand more spectrum channels by over-loading the limited radio spectrum with a large number of devices [6]. Thus, increasing spectrum efficiency is a primary task for IoT networks.

As a remedy, non-orthogonal multiple access (NOMA) has recently gained attention as a key technology to mitigate spectrum scarcity faced by the wireless networks [7].

The primary idea of NOMA is to implement successive interference cancellation (SIC) and allow multiple users to share the same radio resources [8]. The NOMA techniques are mainly categorized into two general classes, i.e., code domain (CD) and power domain (PD) NOMA schemes. The CD-NOMA uses similar codes as in code division multiple access (CDMA) systems and achieves multiplexing gain. In this method, NOMA can utilize sparse or non-orthogonal cross-correlation sequences for each user [9]. On the other hand, in the PD-NOMA, which is considered to be the most prevalent scheme, a source transmits superpositioned messages of all interested users simultaneously; however, each message is assigned with different power level depending on the intended user's QoS level or channel condition [10]. The most well-known performance metrics for generic wireless networks are considered to be the outage probability (OP) and ergodic capacity, which can also be used to analyze performance in IoT networks. Moreover, there are key IoT challenges outlined in the literature, such as mobility, reliability, scalability, performance, security and so on [11]. Improving the OP is crucial in addressing the reliability aspect in IoT networks (as well as the concept of network lifetime [12]) while ensuring capacity is key to address the scalability and performance challenge.

A. RELATED WORKS

The performance of PD-NOMA networks has been analyzed in numerous research works. For instance, uplink NOMA systems were studied in terms of outage analysis in [13], where the authors considered dynamic ordering SIC receivers, while an advanced SIC receiver was proposed in [14]. Meanwhile, other works studied the performance analysis as well, but considering the downlink NOMA systems. For example, the OP and the achievable sum-rate for downlink NOMA systems were analyzed by considering randomly deployed users in [15]. Moreover, the OP of NOMA systems was investigated in [16], where the authors considered statistical channel state information (CSI) with the Nakagami- m channel models. In addition, power-bandwidth allocation and α -fair resource allocation are jointly studied under the assumption of imperfect SIC (ImpSIC) in [17] and [18], accordingly. Moreover, the authors in [19] and [20] studied the security aspects of hybrid automatic repeat request-assisted NOMA networks, where a security-required user is paired with a quality of service (QoS)-sensitive user to establish secure transmission.

1) RELAYING STRATEGIES IN NOMA SYSTEMS

Using relaying strategies in the NOMA networks can provide coverage extension and better reliability for IoT devices with short-range communication [21]–[23]. By leveraging the spectral diversity [24], a source node can improve its transmission range and performance by cooperatively communicating over a relay node. Depending on the relay behavior, there are two widely known relaying protocols, namely, decode-and-forward (DF) and amplify-and-forward (AF). In the DF, the received signal is decoded, re-encoded, and

then forwarded to the next destination, while, the AF first amplifies the received signal and then forwards it to the destination [25]. Recent works on NOMA and cooperative communications can be categorized into two directions: (1) cooperative NOMA, where NOMA users with good channel conditions act as relays to assist those with poor channel conditions; and (2) relay-aided NOMA transmission, where one or more dedicated relays deliver signals to NOMA destination users.

Cooperative NOMA: The authors in [26] showed that the half-duplex (HD) cooperative NOMA outperforms both non-cooperative NOMA and cooperative orthogonal multiple access (OMA) techniques while the OP and ergodic capacity for the similar cooperative NOMA system were studied in [21], where the authors assumed DF relays working in full-duplex (FD) and considered arbitrary and optimal power allocation (PA) methods.

Relay-aided NOMA: The author in [27] derived analytical expressions for the OP and ergodic capacity for two-hop NOMA relaying systems over Rayleigh fading channels considering the HD relay mode, while the same performance metrics with the FD relaying were studied in [28]. Moreover, the outage performance was examined in [29], where a NOMA relaying system considering Nakagami- m fading channels was studied by assuming that the source transmits superimposed signal to multiple destinations with help of AF relay working in the FD regime. The authors considered a relay-aided NOMA network in [23], where the OP is analyzed for different relay selection schemes with multiple HD-DF relays. The advantages of using a relay in NOMA networks also imposed in [30] and [31]. For example, [30] studied a relay-based NOMA system with one transmitter communicating with two receivers via multiple relays employing AF and DF relaying modes, where NOMA nodes were ordered regarding their QoS requirements. Additionally, the cooperative NOMA system was studied in [31], where the authors proposed optimal relay selection schemes considering fixed and adaptive PAs at the relay nodes.

2) COGNITIVE RADIO INSPIRED NOMA SYSTEMS

Another technology that is offered as a solution for the spectrum deficiency problem is cognitive radio (CR) [32], [33]. The main concept of the CR is to provide unlicensed users, a.k.a secondary users (SUs), access to the licensed spectrum bands by avoiding harmful interference to licensed users, a.k.a., primary users (PUs), who are entitled to communicate at those bands. There are three main CR paradigms that allow broadcasting in the primary spectrum bands, i.e., interweave [34], underlay [35] and overlay [36]. In the underlay CR, which is the most popular CR approach, SUs can simultaneously broadcast with the PUs within the same frequency band on the condition that no harmful interference caused to the PUs. Thus, to avoid interference at the primary network, the SUs need to communicate with restricted transmit power, which restrains the SUs to short-range communication. The use of a relay node may allow underlay CR network to expand

their communication links. On the other hand, the underlay CR does not need to sense the entire spectrum band to acquire access to communication, which is the principal advantage of this approach. Thus, the authors in [37] proposed two novel signal-to-noise (SNR) estimation methods for underlay CR-based industrial IoT, which aims are to handle non-data aided SNR estimations for multiple SUs. Moreover, a primary user detection model for CR-IoT using a hidden Markov model was proposed in [38] to improve the delay and throughput of the network.

Lately, the synergy of CR and NOMA technologies showed the capability of obtaining better spectrum efficiency and a significant decrease in the complexity of the power allocation (PA) design [39], [40]. For example, large-scale underlay CR networks with the NOMA scheme was studied in [39] to enhance the connectivity of SUs. The results exposed that thoughtful design of the PA factors and target data rates can show better performance for NOMA users than OMA ones. The authors in [40] studied the overlay paradigm, where the secondary NOMA transmit nodes delivered signal to SUs and helped primary transmitters by relaying their signals to primary destination users.

The benefit of cooperative communications has also been applied in CR-NOMA networks, especially for underlay CR approach, where SUs use short-range communication due to restricted transmit power [32], [41]. Moreover, a relaying node improves the coverage area and throughput of CR networks [42]. In relay-aided CR-NOMA networks, the cognitive network can obtain better throughput by implementing the main two strategies: 1) the cooperation among the PUs and SUs; 2) the cooperation uniquely among the SUs [43]. The authors in [44] compared the performance of licensed and unlicensed bands with that of the conventional relay network. The results showed that adopting cooperation in CR provides outstanding performance in wireless relay networks by reducing inter-cell interference. Also, a novel cooperative multicast CR-NOMA scheme was proposed in [41], where a two-stage cooperative strategy is applied to improve fairness among SUs. Besides, [32] considered a cooperative CR-NOMA network with unicast and multicast communication sessions of the PUs and SUs, respectively, where the cooperation was proposed to improve the outage performance of both PUs and SUs.

3) RESIDUAL TRANSCIEVER HARDWARE IMPAIRMENTS

All the aforementioned studies considered perfect radio frequency (RF) elements at the transceivers. This assumption is not practical as in real-time communication all transceivers experience different types of hardware impairments (HIs) [45], e.g., in-phase/quadrature imbalance, amplifier nonlinearities, quantization error, phase noise, etc. Despite there are exist several algorithms to mitigate the effect of such HIs, some residual transceiver hardware impairments (RTHIs) caused by various kinds of noise and inaccurate calibration can not be eliminated [46]. RTHIs have been examined considering various system models [47]–[51]. For instance,

the authors in [47] showed that the transmit power can not eliminate the influence of RTHIs on the system performance. Meantime, the impact of HIs on NOMA networks was highlighted in [48]. Furthermore, in the context of CR, the authors in [49] investigated the OP of a dual-hop CR system with HIs over Rayleigh fading channels, where it was noted that the AF relaying scheme is less prone to the HIs than DF one. Moreover, a dual-hop relay-aided CR network over the Nakagami- m was examined in [50], where the impact of RTHIs and interference temperature constraint (ITC) on the OP of the system is studied. In real-time communications, it is hardly possible for NOMA users to perform error-free SIC detection. Therefore, the consideration of perfect SIC with all completely canceled interference is highly idealistic [51]. Thus, there is still a lack of research to analyze the impact of RTHIs and ImpSIC on CR-NOMA networks.

B. MOTIVATION AND MAIN CONTRIBUTIONS

Wireless medium is unpredictable, thus, the statistics of the wireless channel can be presented by various distributions. For instance, the long-term signal variation is mostly characterized by the Log-normal distribution and the short-term signal variation can be presented by various other distributions such as Rician, Rayleigh, etc. All the aforementioned studies of CR-NOMA mainly considered Rayleigh and Nakagami- m fading distributions whilst neglecting other distributions, i.e., Log-normal, Negative exponential, Weibull, etc. Therefore, this paper investigates the relay-aided CR-NOMA enabled IoT network using the generalized $\alpha - \mu$ fading distribution and consisting of a primary transmitter and receiver as well as secondary source, relay and K destination users. It is worth pointing out that the joint investigation of CR and NOMA techniques can solve the spectrum shortage and interference issues in IoT networks. Moreover, generalized $\alpha - \mu$ distribution fully covers all the above-mentioned statistical models, namely, Rician, Rayleigh, Nakagami- m , Log-normal, Negative exponential, Weibull, etc. In addition, to consider a more practical system model, the impact of RTHIs and ImpSIC on the performance of the proposed system model will be investigated as well. Different from [51], where the authors studied cooperative NOMA systems over $\alpha - \mu$ distribution without considering interference-limited scenario, we investigate relay-aided underlay CR-NOMA systems considering primary and secondary interference terms.

The key contributions of this work are as follows:

- We derive a novel unified closed-form analytical expression for the end-to-end OP of secondary NOMA users in the underlay CR-NOMA relaying network over the generalized $\alpha - \mu$ statistical model, which provides accurate characterizations of the influence of RTHIs and ImpSIC on the OP of NOMA users. All analytical derivations are validated through Monte Carlo simulations, which verifies the correctness of analytical results. Moreover, the CR-NOMA network is shown to deliver superior per-

formance in comparison with the conventional orthogonal (time-domain) CR relaying network.

- An asymptotic behavior of the system is studied, where the secondary transmit nodes do not cause any interference to the primary network or, in other words, primary users can tolerate any interference generated by the secondary network, i.e., $ITC \rightarrow \infty$. This system model can also be considered as a conventional NOMA network. Furthermore, closed-form expressions for another asymptotic analysis of the OP at high signal-to-noise-ratio (SNR) are obtained to gain more technical insights on the system performance.
- We use a non-homogeneous behavior of $\alpha - \mu$ distribution in the proposed model by considering practical cases, where the CR-NOMA network experiences different channel fading from one time slot to another, i.e., Rayleigh / Nakagami- m , Rayleigh / Weibull, Nakagami- m / Weibull, Nakagami- m / Rayleigh, etc.
- The derived analytical expressions are used to evaluate the impact of several fading and system parameters on the network performance, where results demonstrate that the performance can be improved sufficiently as α and/or μ are/is increased.

C. NOTATIONS AND PAPER ORGANIZATION

Notation: Throughout this paper, $f_{\Psi}(\cdot)$ and $F_{\Psi}(\cdot)$ indicate the probability density function (PDF) and the cumulative distribution function (CDF) of a random variable (RV) Ψ , respectively. $\Pr[\cdot]$ denotes probability and $\mathbb{E}[\cdot]$ is the expectation operator. $\mathcal{CN}(\nu, \sigma^2)$ denotes a complex circularly-symmetric Gaussian distribution with mean ν and variance σ^2 . Also, $\Gamma(a) = \int_0^{\infty} t^{a-1} e^{-t} dt$ [52, (8.310)], $\gamma_{inc}(a, x) = \int_0^x t^{a-1} e^{-t} dt$ [52, (8.350.1)] and $\Gamma(a, x) = \int_x^{\infty} t^{a-1} e^{-t} dt$ [52, (8.350.2)] denote the Gamma function, the lower and upper incomplete Gamma functions, accordingly.

The remainder of the paper is organized as follows. Section II defines the system and channel model of the relay-aided CR-NOMA network while Section III derives new analytical and approximated expressions for the OP metric over non-homogeneous generalized α - μ fading channels. Section IV showcases numerical and simulation results according to the Matlab simulations to verify the accuracy of analytical derivations. Finally, concluding remarks and key findings of the paper are drawn in Section V.

II. SYSTEM AND CHANNEL MODEL

A. SYSTEM TOPOLOGY

A downlink dual-hop CR-NOMA based IoT network is considered as shown in Fig. 1, where a secondary network consists of a source (S), which broadcasts individual messages to IoT devices denoted by D_k , $k \in \mathcal{A} = \{1, 2, \dots, K\}$, via a secondary relay (R) that operates in the HD-DF mode. On the other hand, the primary network consists of a primary transmitter (P_T) and a primary receiver (P_R). All nodes are assumed to be equipped with single antennas.

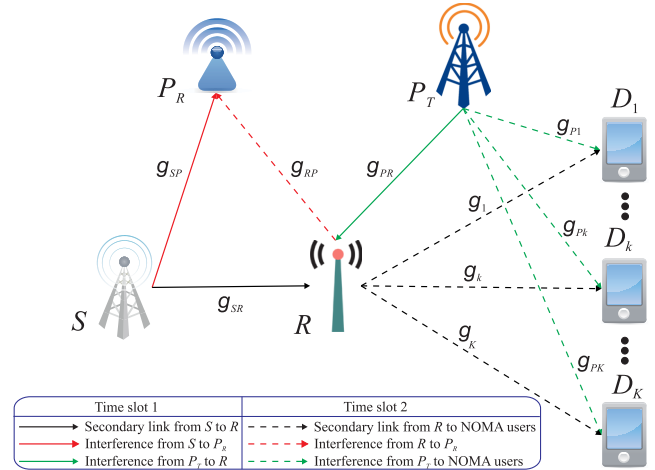


FIGURE 1. The proposed underlay CR-NOMA based IoT network, where the channel links within one time domain follow the same statistical model.

Throughout the paper, we also assume that the CSI estimates stay static or quasi-static and are valid until the following CSI acquisition. All channel links, i.e., g_j , $j \in \mathcal{B} = \{SP, RP, SR, PR, P1, \dots, Pk, \dots, PK, \mathcal{A}\}$, are subject to a quasi-static $\alpha - \mu$ statistical fading model. The respective distances are represented by $d_{j \in \mathcal{B}}$, and τ denotes the path-loss exponent.

The PDF of the channel coefficient g_j for a fading signal with envelope (r) following the α - μ distribution can be written as [53]

$$f_{g_j}(r) = \frac{\alpha_j \mu_j^{\mu_j} r^{\alpha_j \mu_j - 1}}{\hat{r}^{\alpha_j \mu_j} \Gamma(\mu_j)} \exp\left(-\frac{\mu_j}{\hat{r}^{\alpha_j}} r^{\alpha_j}\right), \quad j \in \mathcal{B}, \quad (1)$$

where $\alpha_j > 0$ indicates an arbitrary parameter while \hat{r} stands for the α_j -root mean value given by $\hat{r} = \sqrt[\alpha_j]{\mathbb{E}[r^{\alpha_j}]}$ and $\mu_j \geq \frac{1}{2}$ is the inverse of normalized variance of r^{α_j} given by

$$\mu_j = \frac{\mathbb{E}[r^{\alpha_j}]}{(\mathbb{E}[r^{2\alpha_j}] - \mathbb{E}^2[r^{\alpha_j}])}. \quad (2)$$

Remark 1: Note that the α - μ distribution is the generic fading statistical model that describes small-scale fading channels such as Rayleigh ($\alpha = 2$, $\mu = 1$), Weibull (α is the fading parameter with $\mu = 1$), Nakagami- m (μ is the fading parameter with $\alpha = 2$), etc. [54].

Considering the IoT-based underlay CR paradigm, it is assumed that S and R are restricted with maximum allowed transmit power in order to avoid harmful interference at P_R . Thus, to prevent such interference intervention, the transmit power of secondary transmit node i is restricted as [55]

$$L_i \leq \min\left(\bar{L}_i, \frac{L_{ITC,i} d_{iP}^\tau}{|g_{iP}|^2}\right), \quad i \in \{S, R\}, \quad (3)$$

where \bar{L}_i is the maximum transmit power at node i while $L_{ITC,i}$ is the ITC at P_R caused by node i .

Considering the proposed CR-NOMA relaying model, S transmits a superimposed message $x = \sum_{k=1}^K \sqrt{\rho_k} x_k$ to the

secondary users via R within two time periods, where ρ_k denotes the PA factor of message x_k . Furthermore, different level of transmit power is assigned to each user to properly define each user during the SIC detection, i.e., $\rho_1 > \dots > \rho_k \dots > \rho_K$, with $\sum_{k=1}^K \rho_k = 1$. By doing so, we assume that the communication link of D_K is stronger compared to D_{K-1} , i.e., $g_1 < \dots < g_k \dots < g_K$.

B. TRANSMISSION PROTOCOL

During the 1st time period, R receives the following signal from S

$$y_R = \nabla_S \left(\sum_{k=1}^K \sqrt{\rho_k} x_k + \eta_{SR} \right) g_{SR} + \nabla_P (x_P + \eta_P) g_{PR} + n_R, \quad (4)$$

where $\nabla_i = \sqrt{\frac{L_i}{d_{iR}^\alpha}}$, with $i \in \{S, R\}$, $\eta_{(\cdot)} \sim \mathcal{CN}(0, \varphi_{(\cdot)}^2)$ is the aggregated distortion noise from transceiver; $\varphi_{(\cdot)} = \sqrt{\varphi_t^2 + \varphi_r^2}$ represents the aggregate HI level from the transmitter and receiver. In practice, this level can be measured by the error vector magnitude (EVM) [45]; $n_{(\cdot)} \sim \mathcal{CN}(0, \sigma_{(\cdot)}^2)$ is the additive white Gaussian noise (AWGN) term at each receive node; L_P and x_P are the transmit power and the message of P_T , respectively.

The proposed system model constrained by the RTHIs and interference noises. Considering this, the instantaneous signal-to-noise-distortion-interference ratio (SNDIR) of decoding x_k , with $k \in \{1, \dots, K - 1\}$, at R is written as

$$\gamma_{R,k} = \frac{\rho_k T_S |g_{SR}|^2}{(\tilde{U}_k + \tilde{U}_k + \varphi_{SR}^2) T_S |g_{SR}|^2 + c T_P |g_{PR}|^2 + \sigma_R^2}, \quad (5)$$

where $T_v = \frac{L_v}{d_{vR}^\alpha}$, $v \in \{S, P\}$; $\tilde{U}_k = \sum_{l=1}^{k-1} \vartheta_l \rho_l$, with $0 < \vartheta_l < 1$, where $\vartheta_l = 0$ and $\vartheta_l = 1$ indicate perfect and no SIC, accordingly; $\tilde{U}_k = \sum_{l=k+1}^K \rho_l$, $c = (1 + \varphi_P^2)$ and $\sigma_{(\cdot)}^2$ denotes the AWGN noise variance at each receive node. Now, considering that x_k is decoded under the condition of ImpSIC, the SNDIR of D_K to decode its own message x_K can be written as

$$\gamma_{R,K} = \frac{\rho_K T_S |g_{SR}|^2}{(\tilde{U}_K + \varphi_{SR}^2) T_S |g_{SR}|^2 + c T_P |g_{PR}|^2 + \sigma_R^2}, \quad (6)$$

where $\tilde{U}_K = \sum_{l=1}^{K-1} \vartheta_l \rho_l$.

In the 2nd time period, R broadcasts the decoded superimposed signal $\sum_{k=1}^K \sqrt{b_k} \tilde{x}_k$ to all secondary NOMA users, where b_k , with $\sum_{k=1}^K b_k = 1$, is the PA factor allocated to \tilde{x}_k . Thus, the NOMA user k receives the following signal

$$y_j = \sqrt{\frac{L_R}{d_j^\alpha}} \left(\sum_{k=1}^K \sqrt{b_k} \tilde{x}_k + \eta_j \right) g_j + \sqrt{\frac{L_P}{d_{Pj}^\alpha}} (x_P + \eta_P) g_{Pj} + n_j, \quad (7)$$

Considering ($1 \leq j \leq k \leq K$) and ($b_1 > b_j > b_k > b_K$), D_k applies the SIC to decode the message of D_j using the following SNDIR

$$\gamma_{k,j} = \frac{b_j T_{Rk} |g_k|^2}{(\tilde{U}_j + \tilde{U}_b + \varphi_k^2) T_{Rk} |g_k|^2 + c T_{Pk} |g_{Pk}|^2 + \sigma_k^2}, \quad (8)$$

where $\forall k \in \{1, \dots, K\}$, $T_{uk} = \frac{L_u}{d_{uk}^\alpha}$, with $u \in \{R, P\}$; $\tilde{U}_j = \sum_{l=1}^{j-1} \vartheta_l b_l$ and $\tilde{U}_b = \sum_{l=j+1}^K b_l$. Further, when $K - 1$ secondary NOMA users' messages are decoded, D_K detects its message by

$$\gamma_K = \frac{b_K T_{RK} |g_K|^2}{(\tilde{U}_K + \varphi_K^2) T_{RK} |g_K|^2 + c T_{PK} |g_{PK}|^2 + \sigma_K^2}, \quad (9)$$

where $\tilde{U}_K = \sum_{l=1}^{K-1} \vartheta_l b_l$.

In real-time communication, the use of many NOMA users may not be feasible since the processing complexity of the SIC at receivers raises in a non-linear manner by the increased number of users [26]. Additionally, when the SIC error propagation exists, this complexity becomes more crucial [56]. Thus, for the sake of practicality, further we consider two PD secondary CR-NOMA users, i.e., D_1 and D_2 . Moreover, as it was shown in [57], in interference-limited networks such as large-scale networks, the system performance is mostly influenced by interference [58]. Hence, further, we assume that the AWGN is ignored. Hence, the signal-to-distortion-interference-ratios (SDIRs) of detecting messages of D_1 and D_2 at R in the 1st time period can be respectively written as

$$\gamma_{R,1} = \frac{\rho_1 T_S |g_{SR}|^2}{(\rho_2 + \varphi_{SR}^2) T_S |g_{SR}|^2 + c T_P |g_{PR}|^2}, \quad (10)$$

$$\gamma_{R,2} = \frac{\rho_2 T_S |g_{SR}|^2}{(\vartheta_1 \rho_1 + \varphi_{SR}^2) T_S |g_{SR}|^2 + c T_P |g_{PR}|^2}. \quad (11)$$

Then, in 2nd time period, D_1 decodes its own message with the SDIR of

$$\gamma_1 = \frac{b_1 T_{R1} |g_1|^2}{(b_2 + \varphi_1^2) T_{R1} |g_1|^2 + c T_{P1} |g_{P1}|^2}, \quad (12)$$

Similarly, D_2 first detects \tilde{x}_1 with the SDIR of

$$\gamma_{2,1} = \frac{b_1 T_{R2} |g_2|^2}{(b_2 + \varphi_2^2) T_{R2} |g_2|^2 + c T_{P2} |g_{P2}|^2}. \quad (13)$$

Then, D_2 removes the message of D_1 from (7) and detects its own signal by the following SDIR

$$\gamma_2 = \frac{b_2 T_{R2} |g_2|^2}{(\vartheta_1 b_1 + \varphi_2^2) T_{R2} |g_2|^2 + c T_{P2} |g_{P2}|^2}. \quad (14)$$

Finally, the achievable data rate at D_j can be given as

$$\mathcal{R}_j = \frac{1}{2} \log_2 \left(1 + \min(\gamma_{R,j}, \gamma_j) \right), \quad j \in \{1, 2\}, \quad (15)$$

where the factor $\frac{1}{2}$ implies that two time periods are required.

III. OUTAGE PERFORMANCE

In this section, the exact OP for D_1 and D_2 is derived. The OP of D_j is defined as the probability that the data rate achievable by D_j is below a predefined target rate $\mathcal{R}_{th,j}$, i.e.,

$$P_{out,j} = \Pr[\mathcal{R}_j < \mathcal{R}_{th,j}]. \quad (16)$$

The OP of D_1 can be expressed using (10), (12) and (15) as

$$\begin{aligned} P_{out,1}(\theta_1) &= \Pr[\min(\gamma_{R,1}, \gamma_1) < \theta_1] \\ &= 1 - \Pr[\min(\gamma_{R,1}, \gamma_1) > \theta_1] \\ &= 1 - \Pr[\gamma_{R,1} > \theta_1] \Pr[\gamma_1 > \theta_1] \\ &= 1 - (1 - \Pr[\gamma_{R,1} < \theta_1]) (1 - \Pr[\gamma_1 < \theta_1]) \\ &= F_{\gamma_{R,1}}(\theta_1) + F_{\gamma_1}(\theta_1) - F_{\gamma_{R,1}}(\theta_1)F_{\gamma_1}(\theta_1), \quad (17) \end{aligned}$$

where $\theta_i = 2^{2\mathcal{R}_{th,i}} - 1$ is the SNR associated with the rate threshold of D_i .

The CDF of the RV $\gamma_{R,1}$, considering the ITC at P_R , can be written as in (18), shown at the bottom of this page, where $X = |g_{SR}|^2$, $Y = |g_{SP}|^2$, $Z = |g_{PR}|^2$, $\bar{I}_{SP} = L_{ITC}d_{SP}^\tau$, $\Delta_1 = \frac{(1+\varphi_p^2)T_P\theta_1}{T_S(\rho_1 - [\rho_2 + \varphi_{SR}^2]\theta_1)}$, $\Delta_2 = \frac{(1+\varphi_p^2)T_P\theta_1 d_{SR}^\tau}{\bar{I}_{SP}(\rho_1 - [\rho_2 + \varphi_{SR}^2]\theta_1)}$ and $\Lambda = \frac{\bar{I}_{SP}}{L_S}$.

$$\begin{aligned} F_{\gamma_{R,1}}(\theta_1) &= 1 - \frac{\lambda_z^{\mu_z} \gamma_{inc}(\mu_y, \lambda_y \Lambda^{\frac{\alpha}{2}})}{\Gamma(\mu_y)\Gamma(\mu_z)} \\ &\times \sum_{m=0}^{\mu_x-1} \frac{\lambda_x^m \Delta_1^{\frac{\alpha m}{2}} \Gamma(\mu_z + m)}{m! (\lambda_z + \lambda_x \Delta_1^{\frac{\alpha}{2}})^{\mu_z+m}} \\ &- \frac{\lambda_z^{\mu_z} \lambda_y^{\mu_y} e^{-\lambda_y \Lambda^{\frac{\alpha}{2}}} \Delta_2^{-\frac{\alpha \mu_z}{2}}}{\lambda_x^{\mu_x} \Gamma(\mu_y)\Gamma(\mu_z)} \\ &\times \sum_{m_2=0}^{\mu_x-1} \sum_{i=0}^{\mu_y+m_2-1} \sum_{s=0}^i \binom{i}{s} \frac{\lambda_y^i \Lambda^{\frac{\alpha i}{2}}}{m_2! i!} \\ &\times G_{1,2}^{2,1} \left(\left. \frac{(\lambda_z + \lambda_x [\Lambda \Delta_2]^{\frac{\alpha}{2}})}{\lambda_y^{-1} \lambda_x \Delta_2^{\frac{\alpha}{2}}} \right| \begin{matrix} 1 - (\mu_z + m_2 + s) \\ 0, -\mu_z + \mu_y - s \end{matrix} \right) \quad (19) \end{aligned}$$

A. EXACT OUTAGE PROBABILITY

Proposition 1: The CDF of $\gamma_{R,1}$ in (18) can be written in a closed-form as in (19).

Proof: See Appendix A. ■

Similarly, using (12), the CDF of the RV γ_1 can be described as

$$\begin{aligned} F_{\gamma_1}(\theta_1) &= \Pr[\gamma_1 < \theta_1] = \Pr[Q < W\Phi_1, U < \Lambda_1] \\ &+ \Pr[Q < UW\Phi_2, U > \Lambda_1], \quad (20) \end{aligned}$$

$\underbrace{\hspace{10em}}_C$
 $\underbrace{\hspace{10em}}_D$

where $Q = |g_1|^2$, $U = |g_{RP}|^2$, $W = |g_{P1}|^2$, $\bar{I}_{RP} = L_{ITC}d_{RP}^\tau$, $\Phi_1 = \frac{(1+\varphi_p^2)T_{P1}\theta_1}{T_{R,1}(b_1 - [b_2 + \varphi_1^2]\theta_1)}$, $\Phi_2 = \frac{(1+\varphi_p^2)T_{P1}d_1^\tau}{\bar{I}_{RP}(b_1 - [b_2 + \varphi_1^2]\theta_1)}$ and $\Lambda_1 = \frac{\bar{I}_{RP}}{L_R}$. Now, following the same step as in Appendix A, the CDF of γ_1 can be written in closed-form, as in (21), shown at the bottom of the next page, where $\theta_1 < \frac{b_1}{b_2 + \varphi_1^2}$, otherwise, $F_{\gamma_1}(\theta_1) \sim 1$.

Finally, by substituting (19) and (21) into (17) and after some algebraic manipulations, the exact OP of D_1 can be derived in its closed-form as in (23), shown on the next page.

The outage metric of D_2 can be calculated using Eqs. (11), (14) and (15) as

$$\begin{aligned} P_{out,2}(\theta_2) &= \Pr[\min(\gamma_{R,2}, \gamma_2) < \theta_2] \\ &= F_{\gamma_{R,2}}(\theta_2) + F_{\gamma_2}(\theta_2) - F_{\gamma_{R,2}}(\theta_2)F_{\gamma_2}(\theta_2). \quad (22) \end{aligned}$$

Furthermore, by following the same procedure in obtaining the OP of D_1 , the closed-form OP for D_2 can be written as in (24), shown on the next page, where $V = |g_2|^2$, $H = |g_{P2}|^2$, $\Upsilon_1 = \frac{(1+\varphi_p^2)T_P\theta_2}{T_S(\rho_2 - [\varrho_1\rho_1 + \varphi_{SR}^2]\theta_2)}$, $\Upsilon_2 = \frac{(1+\varphi_p^2)T_P\theta_2 d_{SR}^\tau}{(1+\varphi_p^2)T_{P2}\theta_2}$, $\aleph_1 = \frac{(1+\varphi_p^2)T_{P2}\theta_2}{T_{R,2}(b_2 - [\varrho_1 b_1 + \varphi_2^2]\theta_2)}$, $\aleph_2 = \frac{L_{ITC}d_{SP}^\tau(\rho_2 - [\varrho_1\rho_1 + \varphi_{SR}^2]\theta_2)}{(1+\varphi_p^2)T_{P2}\theta_2 d_2^\tau}$ and $\theta < \frac{\chi_2}{\varrho_1\chi_1 + \varphi_{SR}^2}$, with $\chi \in \{\rho, b\}$.

Using (15) and (23) or (24), the average throughput of D_j is written as

$$C_j = \mathcal{R}_j(1 - P_{out,j}), \quad j \in \{1, 2\}. \quad (25)$$

B. ASYMPTOTIC ANALYSIS

In this section, we investigate the asymptotic behavior of the considered system model. First of all, we study a certain asymptotic case with a high SNR regime, i.e., $\{L_S; L_R\} \rightarrow \infty$, to understand the impact of the ITC on the outage performance of non-homogeneous fading parameters of the system. Therefore, considering the high SNR regime, the ITC becomes the dominant factor to determine the maximum

$$\begin{aligned} F_{\gamma_{R,1}}(\theta_1) &= \Pr[\gamma_{R,1} < \theta_1] = \Pr \left[\frac{\rho_1 T_S |g_{SR}|^2}{(\rho_2 + \varphi_{SR}^2) T_S |g_{SR}|^2 + cT_P |g_{PR}|^2} < \theta_1, \bar{L}_S < \frac{\bar{I}_{SP}}{|g_{SP}|^2} \right] \\ &+ \Pr \left[\frac{\rho_1 \bar{I}_{SP} |g_{SR}|^2}{(\rho_2 + \varphi_{SR}^2) \frac{\bar{I}_{SP}}{d_{SR}^\tau} |g_{SP}|^2 + cT_P |g_{PR}|^2} < \theta_1, \bar{L}_S > \frac{\bar{I}_{SP}}{|g_{SP}|^2} \right] \\ &= \underbrace{\Pr[X < Z\Delta_1, Y < \Lambda]}_A + \underbrace{\Pr[X < YZ\Delta_2, Y > \Lambda]}_B, \quad (18) \end{aligned}$$

allowed transmit power at S and R ; hence, a fixed L_{ITC} will limit the use of excessive power at secondary transmitters. Thus, considering the above assumption, the maximum allowed transmit power of S and R in (3) can be rewritten as

$$L_i \leq \frac{L_{ITC} d_{iP}^r}{|g_{iP}|^2}, \quad i \in \{S, R\}. \quad (26)$$

Therefore, considering these new reformulated power constraints, we can write the high SNR asymptotic outage performance of D_1 and D_2 as in (27) and (28), respectively. We refer

interested readers to Appendix B for the derivation steps.

$$P_{out,1}^{HS}(\theta_1) = \frac{\lambda_x^{\mu_x} \Delta_2^{\frac{\alpha\mu_x}{2}} \Gamma(\mu_x + \mu_y) \Gamma(\mu_x + \mu_z)}{\lambda_y^{\mu_x} \lambda_z^{\mu_x} \mu_x \Gamma(\mu_x) \Gamma(\mu_y) \Gamma(\mu_z)} + \frac{\lambda_q^{\mu_q} \Phi_2^{\frac{\alpha_2\mu_q}{2}} \Gamma(\mu_q + \mu_u) \Gamma(\mu_q + \mu_w)}{\lambda_u^{\mu_q} \lambda_w^{\mu_q} \mu_q \Gamma(\mu_q) \Gamma(\mu_u) \Gamma(\mu_w)} - \frac{\lambda_x^{\mu_x} \Delta_2^{\frac{\alpha\mu_x}{2}} \Gamma(\mu_x + \mu_y) \Gamma(\mu_x + \mu_z)}{\lambda_y^{\mu_x} \lambda_z^{\mu_x} \mu_x \Gamma(\mu_x) \Gamma(\mu_y) \Gamma(\mu_z)} \times \frac{\lambda_q^{\mu_q} \Phi_2^{\frac{\alpha_2\mu_q}{2}} \Gamma(\mu_q + \mu_u) \Gamma(\mu_q + \mu_w)}{\lambda_u^{\mu_q} \lambda_w^{\mu_q} \mu_q \Gamma(\mu_q) \Gamma(\mu_u) \Gamma(\mu_w)} \quad (27)$$

$$F_{\gamma_1}(\theta_1) = 1 - \frac{\lambda_w^{\mu_w} \gamma_{inc} \left(\mu_u, \lambda_u \Lambda_1^{\frac{\alpha_2}{2}} \right)}{\Gamma(\mu_u) \Gamma(\mu_w)} \sum_{k=0}^{\mu_q-1} \frac{\lambda_q^{\mu_w} \Phi_1^{\frac{\alpha_2 k}{2}} \Gamma(\mu_w + k)}{k! \left(\lambda_w + \lambda_q \Phi_1^{\frac{\alpha_2}{2}} \right)^{\mu_w+k}} - \frac{\lambda_w^{\mu_w} \lambda_u^{\mu_w} e^{-\lambda_u \Lambda_1^{\frac{\alpha_2}{2}}} \Phi_2^{-\frac{\alpha_2\mu_w}{2}}}{\lambda_q^{\mu_w} \Gamma(\mu_u) \Gamma(\mu_w)} \times \sum_{k_2=0}^{\mu_q-1} \sum_{j=0}^{\mu_u+k_2-1} \sum_{l=0}^j \binom{j}{l} \frac{\lambda_u^j \Lambda_1^{\frac{\alpha_2 j}{2}}}{k_2! j!} G_{1,2}^{2,1} \left(\left(\frac{\lambda_w + \lambda_q [\Lambda_1 \Phi_2]^{\frac{\alpha_2}{2}}}{\lambda_u^{-1} \lambda_q \Phi_2^{\frac{\alpha_2}{2}}} \right) \middle| 1 - (\mu_w + k_2 + l) \right) \quad (21)$$

$$P_{out,1}(\theta_1) = 1 - \left[\frac{\lambda_z^{\mu_z} \gamma_{inc} \left(\mu_y, \lambda_y \Lambda^{\frac{\alpha}{2}} \right)}{\Gamma(\mu_y) \Gamma(\mu_z)} \sum_{m=0}^{\mu_x-1} \frac{\lambda_x^m \Delta_1^{\frac{\alpha m}{2}} \Gamma(\mu_z + m)}{m! \left(\lambda_z + \lambda_x \Delta_1^{\frac{\alpha}{2}} \right)^{\mu_z+m}} + \frac{\lambda_z^{\mu_z} \lambda_y^{\mu_z} e^{-\lambda_y \Lambda^{\frac{\alpha}{2}}} \Delta_2^{-\frac{\alpha\mu_z}{2}}}{\lambda_x^{\mu_z} \Gamma(\mu_y) \Gamma(\mu_z)} \sum_{m_2=0}^{\mu_x-1} \sum_{i=0}^{\zeta-1} \sum_{s=0}^i \binom{i}{s} \frac{\lambda_y^i \Lambda^{\frac{\alpha i}{2}}}{m_2! i!} \times G_{1,2}^{2,1} \left(\left(\frac{\lambda_z + \lambda_x [\Lambda \Delta_2]^{\frac{\alpha}{2}}}{\lambda_y^{-1} \lambda_x \Delta_2^{\frac{\alpha}{2}}} \right) \middle| 1 - (\mu_x + m_2 + s) \right) \right] \left[\frac{\lambda_w^{\mu_w} \gamma_{inc} \left(\mu_u, \lambda_u \Lambda_1^{\frac{\alpha_2}{2}} \right)}{\Gamma(\mu_u) \Gamma(\mu_w)} \sum_{k=0}^{\mu_q-1} \frac{\lambda_q^k \Phi_1^{\frac{\alpha_2 k}{2}} \Gamma(\mu_w + k)}{k! \left(\lambda_w + \lambda_q \Phi_1^{\frac{\alpha_2}{2}} \right)^{\mu_w+k}} + \frac{\lambda_w^{\mu_w} \lambda_u^{\mu_w} e^{-\lambda_u \Lambda_1^{\frac{\alpha_2}{2}}} \Phi_2^{-\frac{\alpha_2\mu_w}{2}}}{\lambda_q^{\mu_w} \Gamma(\mu_u) \Gamma(\mu_w)} \sum_{k_2=0}^{\mu_q-1} \sum_{j=0}^{\mu_u+k_2-1} \sum_{l=0}^j \binom{j}{l} \frac{\lambda_u^j \Lambda_1^{\frac{\alpha_2 j}{2}}}{k_2! j!} G_{1,2}^{2,1} \left(\left(\frac{\lambda_w + \lambda_q [\Lambda_1 \Phi_2]^{\frac{\alpha_2}{2}}}{\lambda_u^{-1} \lambda_q \Phi_2^{\frac{\alpha_2}{2}}} \right) \middle| 1 - (\mu_w + k_2 + l) \right) \right] \quad (23)$$

$$P_{out,2}(\theta_2) = 1 - \left[\frac{\lambda_z^{\mu_z} \gamma_{inc} \left(\mu_y, \lambda_y \Lambda^{\frac{\alpha}{2}} \right)}{\Gamma(\mu_y) \Gamma(\mu_z)} \sum_{m=0}^{\mu_x-1} \frac{\lambda_x^m \Upsilon_1^{\frac{\alpha m}{2}} \Gamma(\mu_z + m)}{m! \left(\lambda_z + \lambda_x \Upsilon_1^{\frac{\alpha}{2}} \right)^{\mu_z+m}} + \frac{\lambda_z^{\mu_z} \lambda_y^{\mu_z} e^{-\lambda_y \Lambda^{\frac{\alpha}{2}}} \Upsilon_2^{-\frac{\alpha\mu_z}{2}}}{\lambda_x^{\mu_z} \Gamma(\mu_y) \Gamma(\mu_z)} \sum_{m_2=0}^{\mu_x-1} \sum_{i=0}^{\zeta-1} \sum_{s=0}^i \binom{i}{s} \frac{\lambda_y^i \Lambda^{\frac{\alpha i}{2}}}{m_2! i!} \times G_{1,2}^{2,1} \left(\left(\frac{\lambda_z + \lambda_x [\Lambda \Upsilon_2]^{\frac{\alpha}{2}}}{\lambda_y^{-1} \lambda_x \Upsilon_2^{\frac{\alpha}{2}}} \right) \middle| 1 - (\mu_z + m_2 + s) \right) \right] \left[\frac{\lambda_h^{\mu_h} \gamma_{inc} \left(\mu_u, \lambda_u \Lambda_1^{\frac{\alpha_2}{2}} \right)}{\Gamma(\mu_u) \Gamma(\mu_h)} \sum_{k=0}^{\mu_v-1} \frac{\lambda_v^k \aleph_1^{\frac{\alpha_2 k}{2}} \Gamma(\mu_h + k)}{k! \left(\lambda_h + \lambda_v \aleph_1^{\frac{\alpha_2}{2}} \right)^{\mu_h+k}} + \frac{\lambda_h^{\mu_h} \lambda_u^{\mu_h} e^{-\lambda_u \Lambda_1^{\frac{\alpha_2}{2}}} \aleph_2^{-\frac{\alpha_2\mu_h}{2}}}{\lambda_v^{\mu_h} \Gamma(\mu_u) \Gamma(\mu_h)} \times \sum_{k_2=0}^{\mu_v-1} \sum_{j=0}^{\mu_u+k_2-1} \sum_{l=0}^j \binom{j}{l} \frac{\lambda_u^j \Lambda_1^{\frac{\alpha_2 j}{2}}}{k_2! j!} G_{1,2}^{2,1} \left(\left(\frac{\lambda_h + \lambda_v [\Lambda_1 \aleph_2]^{\frac{\alpha_2}{2}}}{\lambda_u^{-1} \lambda_v \aleph_2^{\frac{\alpha_2}{2}}} \right) \middle| 1 - (\mu_h + k_2 + l) \right) \right] \quad (24)$$

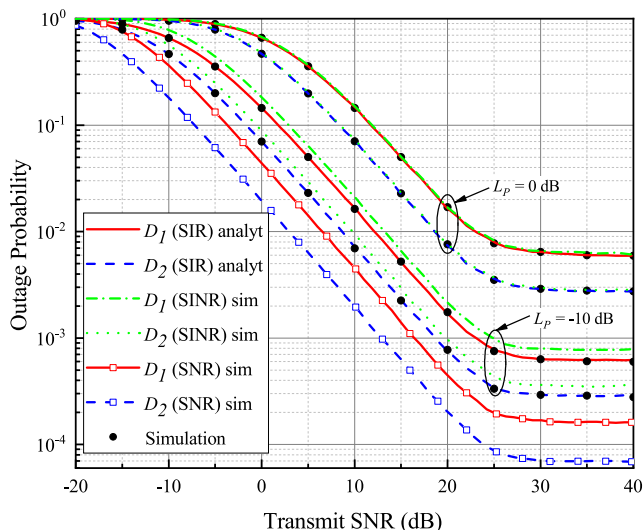


FIGURE 2. The OP vs. the transmit SNR for the Rayleigh distribution ($\alpha = 2$; $\mu = 1$) with $L_p = \{-10, 0\}$ dB.

$$\begin{aligned}
 P_{\text{out},2}^{\text{HS}}(\theta_2) = & \frac{\lambda_x^{\mu_x} \gamma_2^{\frac{\alpha\mu_x}{2}} \Gamma(\mu_x + \mu_y) \Gamma(\mu_x + \mu_z)}{\lambda_y^{\mu_x} \lambda_z^{\mu_x} \mu_x \Gamma(\mu_x) \Gamma(\mu_y) \Gamma(\mu_z)} \\
 & + \frac{\lambda_u^{\mu_v} \delta_2^{\frac{\alpha\mu_v}{2}} \Gamma(\mu_v + \mu_u) \Gamma(\mu_v + \mu_h)}{\lambda_u^{\mu_v} \lambda_h^{\mu_v} \mu_v \Gamma(\mu_v) \Gamma(\mu_u) \Gamma(\mu_h)} \\
 & - \frac{\lambda_x^{\mu_x} \gamma_2^{\frac{\alpha\mu_x}{2}} \Gamma(\mu_x + \mu_y) \Gamma(\mu_x + \mu_z)}{\lambda_y^{\mu_x} \lambda_z^{\mu_x} \mu_x \Gamma(\mu_x) \Gamma(\mu_y) \Gamma(\mu_z)} \\
 & \times \frac{\lambda_u^{\mu_v} \delta_2^{\frac{\alpha\mu_v}{2}} \Gamma(\mu_v + \mu_u) \Gamma(\mu_v + \mu_h)}{\lambda_u^{\mu_v} \lambda_h^{\mu_v} \mu_v \Gamma(\mu_v) \Gamma(\mu_u) \Gamma(\mu_h)} \quad (28)
 \end{aligned}$$

Moreover, it is reasonable to consider another asymptotic behavior of the system when the secondary transmit nodes do not cause any interference to the PN or, in other words, a PU can tolerate any interference generated by the SN, i.e., $L_{\text{ITC}} \rightarrow \infty$ or no ITC imposed. Thus, the power restrictions in (3) are simplified to $L_i \leq \bar{L}_i$, $i \in \{S, R\}$, i.e., there are no power limits at the secondary transmitter i . Then, the derivations of corresponding outage metrics for D_1 and D_2 are shown in Appendix C.

IV. RESULTS DISCUSSION

This section presents numerical results to validate the analytical expressions derived above and provides thorough scrutiny of the impact of different system and fading parameters on the outage performance of the proposed system. The simulation parameters are as follows. The fixed PA factors are considered, if it is not stated otherwise, as $\rho_1 = b_1 = 0.8$ and $\rho_2 = b_2 = 0.2$. Moreover, for simplicity, we assume the same transmit power levels at the secondary transmit nodes, i.e., $L = L_S = L_R$, and the SNR threshold as $\theta_1 = \theta_2 = \theta = 3$ dB. The rest system parameters are shown in Table 1.

Fig. 2 compares the analytical SIR-based OP derived in Section III with the simulation results obtained using SINR in (5), and SNR (using the same equation, but considering

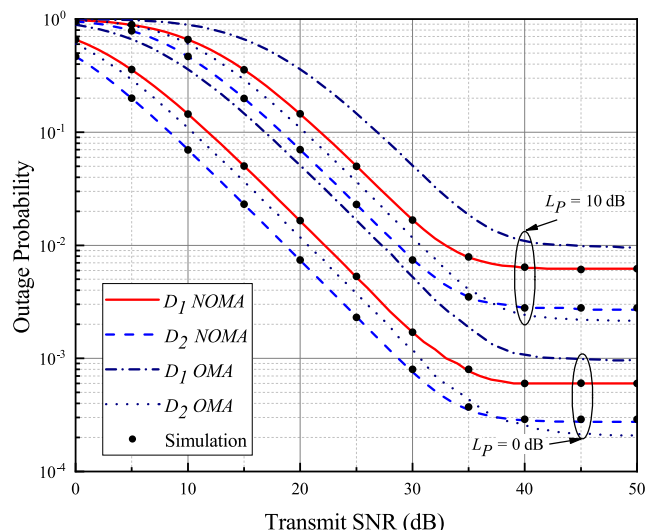


FIGURE 3. The OP comparison of the OMA and NOMA for Rayleigh fading with $L_p = \{0, 10\}$ dB and $L_{\text{ITC}} = 20$ dB.

interference-free regime). As we can see, in all cases, the outage performance of D_2 is superior compared to D_1 which can be explained by the impact of selected system parameters defined in Table 1. Regarding the SIR- versus SNR-based OP comparison, it shows that the OP of NOMA users degrades as the primary interference power level increases. For example, when the transmit SNR = 10 dB, D_1 obtains the OP of 0.01632 for the SNR-based system, while, for the SIR-based one, D_1 achieves 0.02064 and 0.1449 when $L_p = -10$ dB and $L_p = 0$, respectively. Then, when we compare SIR-versus SINR-based system, it is noticed that there is a small OP degradation for the SIR-based system at low interference power level, i.e., $L_p = -10$ dB. However, when $L_p = 0$ dB, the SIR- and SINR-based outage performance show the same results for all transmit SNR regions, which justifies the assumption made in Section III. Finally, it is also important to highlight that the analytical results perfectly coincide with the Monte Carlo simulations in this and forthcoming figures, which validates the accuracy of analytical derivations.

Fig. 3 demonstrates the OP comparison of the analytical CR-NOMA based IoT network with simulated CR-TDMA one. The proposed relay-aided CR-NOMA system requires two-time slots to convey messages to two NOMA-based IoT devices, whilst the TDMA-based model needs four-time slots to provide communication to the same users. Hence, for the purpose of a fair comparison of two systems, we consider the following system parameters for the TDMA system: 1) the data requirement is set as bi-fold of that for the NOMA model; 2) the transmit power at S and R is equal to $0.5L$. As Fig. 3 shows, both NOMA IoT devices of CR-NOMA outperform the TDMA ones in terms of the OP. Noticeably, the outage saturation for NOMA-based IoT devices begins at lower transmit SNR levels compared to those for the TDMA users. This happens due to (3), where transmit power of $0.5L$ rises the values of the ITC at P_R , as a result, the level of transmit SNR where the OP curves start to saturate increases.

TABLE 1. Simulation parameters, where d is assumed to be unity in order to focus on the OP results.

Parameter	Value	Parameter	Value
The S -to- P_R distance, d_{SP}	$3d$	The P_T -to- R distance, d_{PR}	$3d$
The S -to- R distance, d_{SR}	d	The P_T -to- D_1 distance, d_{P1}	$3d$
The R -to- P_R distance, d_{RP}	$3d$	The P_T -to- D_2 distance, d_{P2}	$3d$
The R -to- D_1 distance, d_1	$\{1.5d, 2d, 3d\}$	Path-loss exponent, τ	3
The R -to- D_2 distance, d_2	d	The ITC, $L_{ITC,S} = L_{ITC,R} = L_{ITC}$	$\{10, 20\}$ dB
Compound HI level, $\psi = \psi_{SR} = \psi_1 = \psi_2$	0.1	Imperfect SIC coefficient, ϑ	0.1

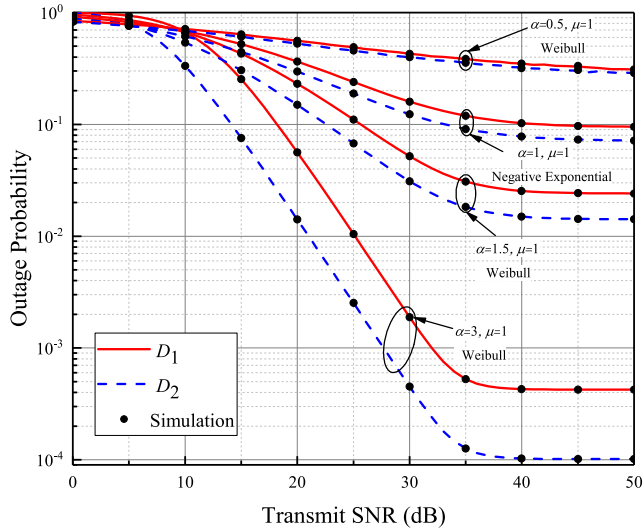


FIGURE 4. The OP over the Weibull ($\mu = 1$) and Negative Exponential ($\alpha = 1; \mu = 1$) distributions with $L_P = 10$ dB and $L_{ITC} = 20$ dB.

Fig. 4 illustrates OP results for the Weibull ($\mu = 1$) distribution and, its special case, Negative Exponential distribution by setting $\alpha = 1$ and fixed $\mu = 1$. Similar to other OP results, D_2 obtains better OP than D_1 . It is also noticed that the increase of the α value helps to obtain better OP. For example, when $\alpha = \{3, 1.5, 1\}$, D_2 achieves the OP of 10^{-1} at 15 dB, 22.5 dB and 32 dB, respectively. The worse OP result is shown by the Weibull curve with $\alpha = 0.5$, where the OP starts to saturate after the OP of 0.5.

In Fig. 5, we evaluate the effect of the ITC on the OP versus the transmit SNR over Nakagami- m fading channels. We consider two scenarios: $L_{ITC} = 10$ dB and $L_{ITC} = 20$ dB. The plot shows that the higher value of the ITC, i.e., $L_{ITC} = 20$ dB, allows achieving better OP performance for the CR-NOMA-based IoT devices, while the lower value of the ITC degrades the OP by starting its saturation at lower transmit SNR levels. Moreover, these saturation curves coincide with the high SNR approximations of the OP performance given by (27) and (28). Besides, we plot asymptotic case with no ITC, i.e., $L_{ITC} \rightarrow \infty$, and this mode shows the best outage performance with no OP curve saturation.

In Fig. 6, we illustrate the average throughput obtained from (25). Similarly to the outage performance, primary interference degrades the performance of an average throughput. The larger value of L_P results in the lower achieved average throughput. Regarding the performance of two CR-NOMA-based IoT devices, it is noticed that D_2 shows a better average

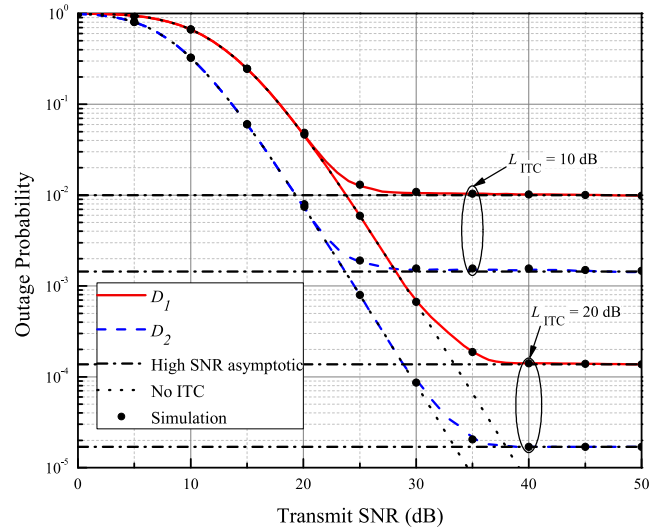


FIGURE 5. The OP vs. the transmit SNR over the Nakagami- m distribution with $L_P = 10$ dB and $L_{ITC} = \{10, 20\}$ dB.

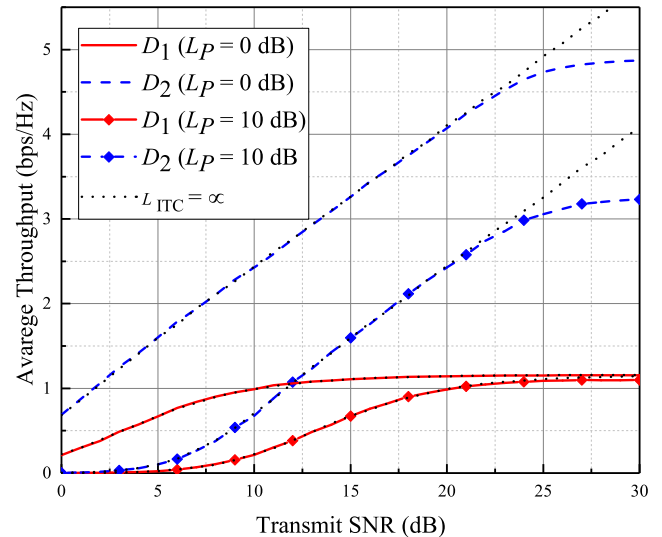


FIGURE 6. The average throughput vs. the transmit SNR over the Nakagami- m distribution with $\rho_1 = 0.8$ and $d_1 = 2d$.

throughput performance than D_1 . For example, in the case of $L_P = 0$ dB and the transmit SNR of 30 dB, D_2 gains the highest average throughput of 4.8 bps/Hz and 5.7 bps/Hz when $L_{ITC} = 10$ dB and $L_{ITC} \rightarrow \infty$, respectively. However, for D_1 , the saturation of the average throughput curves starts at moderate transmit SNR levels even for $L_{ITC} \rightarrow \infty$ mode. This can be explained by the next. Regarding (10) and (12),

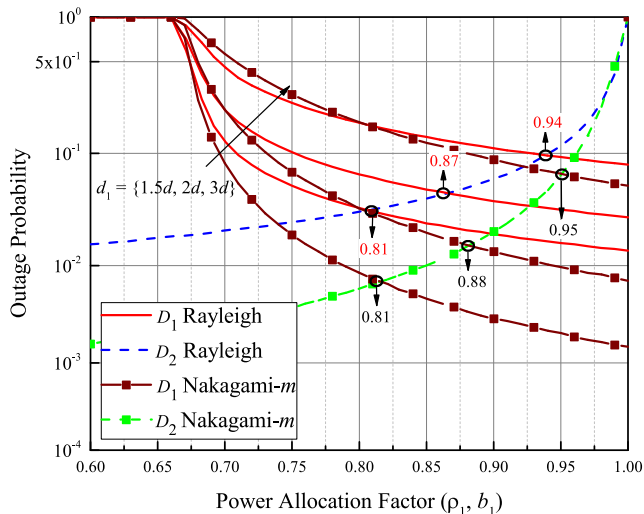


FIGURE 7. The OP of NOMA users vs. PA factor over Rayleigh and Nakagami- m channels at transmit SNR of 20 dB.

TABLE 2. The OF-based PA factors for different d_1 .

Fading type / distance d_1		1.5d	2d	3d
Rayleigh ($\alpha = 2; \mu = 1$)	ρ_1, b_1	0.81	0.87	0.94
	ρ_2, b_2	0.19	0.13	0.06
Nakagami- m ($\alpha = 2; \mu = m = 2$)	ρ_1, b_1	0.81	0.88	0.95
	ρ_2, b_2	0.19	0.12	0.05

the SIR of D_1 has the message of D_2 as interference in its denominator. Thus, when the transmit power is increased, primary interference becomes to be neglectable and the SIR is independent on the transmit power and dependant on $\frac{\alpha_1}{\alpha_2}$. This fact results in the average throughput curve saturation.

Fig. 7 demonstrates simulated results on the PA factors based on the NOMA users' outage fairness (OF) over Rayleigh ($\alpha = 2; \mu = 1$) and Nakagami- m ($\alpha = 2; \mu = 2$) considering system parameters of the transmit SNR = 20 dB, $L_{ITC} = 10$ dB and $L_P = 10$ dB. It is observed that, for all d_1 values, the OP of D_1 is in an outage when $\theta > \frac{\rho_1}{\rho_2}$. However, when $\theta < \frac{\rho_1}{\rho_2}$, the OP of D_1 improves by increasing α_1 values, while that of D_2 decreases. All the OF-based PA factors derived from this figure are demonstrated in Table 2.

In Fig. 8, we present the results on the OP vs. the predefined SNR threshold using OF-based PA factors shown in Table 2 with the transmit SNR of 20 dB, $L_{ITC} = 10$ dB and $L_P = 10$ dB. The figure shows that the outage of D_1 , for all d_1 values, improves when the OF-based PA factors are considered. Especially, when the predefined SNR threshold is equal to 3 dB, the performance of both devices are the same as this SNR threshold value was considered for the PA optimization in Fig. 7. Therefore, it can be stated that OF-based PA factors can provide OF for both IoT devices.

Fig. 9 investigates the impact of the fading parameters α and μ on the OP of D_1 . Here, we define the set of parameters that fully cover all possible system setup variations to evaluate the impact of α and μ . Hence, the channel links in each domain defined in Remark 2 and shown in Fig. 1 are defined as $[(\alpha, \mu_x, \mu_y, \mu_z), (\alpha_2, \mu_q, \mu_u, \mu_w)]$. The first two OP curves shown in the legend of the figure correspond to the

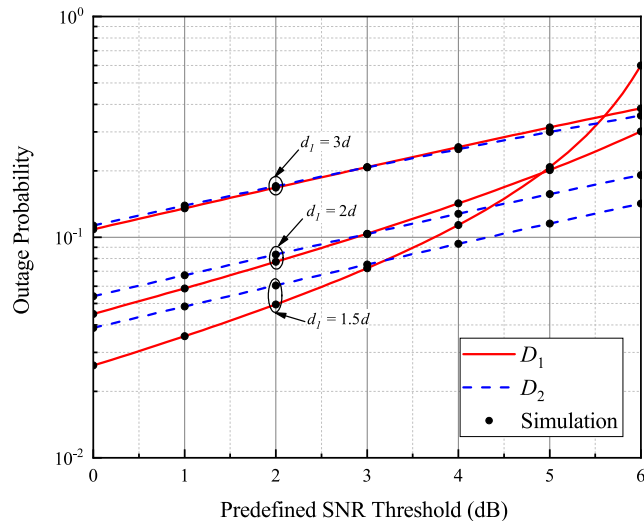


FIGURE 8. The OP of NOMA users vs. the SNR threshold with OF-based PA factors at transmit SNR of 20 dB.

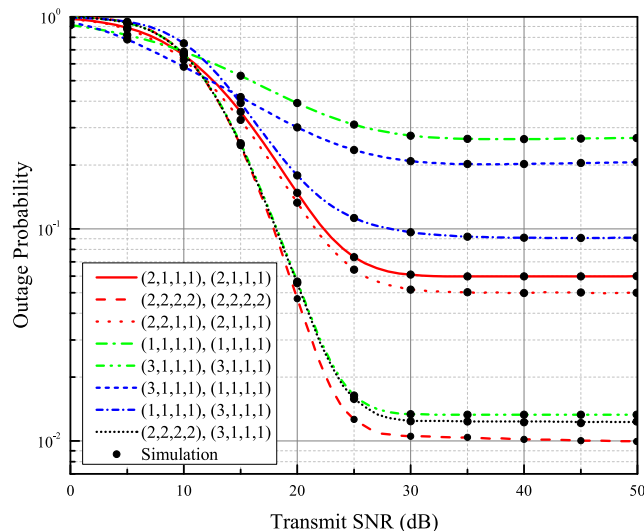


FIGURE 9. The OP of D_1 vs. the transmit SNR for different α and μ parameters when $L_P = 10$ dB and $L_{ITC} = 10$ dB.

channel links following the Nakagami- m distribution ($\mu = 1$ (i.e., Rayleigh) and $\mu = 2$) with identical μ parameters per the system setup. It is perceived that the smaller value of μ degrades the OP of the system as μ depicts the number of multi-path components of the channel. Next, we consider the system setup with $[(2, 2, 1, 1), (2, 1, 1, 1)]$ to support our aforementioned statement. As a result, we can see that the OP of D_1 improves respectively. Further, various system setups regarding the Weibull statistical model are considered. For example, curves with different α values (green lines) show that bigger α results in better outage performance. This can be explained by the fact that the fading parameter is related to the power exponent of the channel. To justify this statement, we set $\alpha = 3$ (blue lines) and both system models outperform the first green line in means of the outage performance. Finally, the OP results related to the system is demonstrated considering the setup when the channel links in each domain follow two different fading models, i.e., Nakagami- m

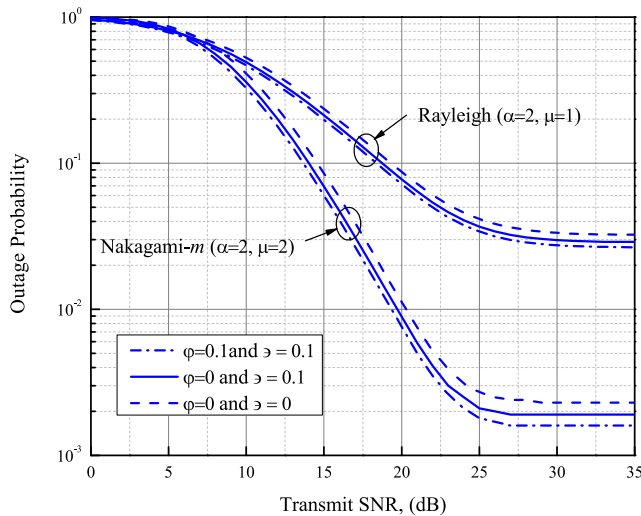


FIGURE 10. The OP of NOMA users vs. the transmit SNR for ImpSIC and RTHIs when $L_p = 10$ dB and $L_{ITC} = 10$ dB.

(with $\mu = 2$) and Weibull (with $\alpha = 3$). Another useful insight is that μ has higher impact on the outage than that of α . It can be found by comparing this line with the second OP curve (dashed red), that the latter obtains better outage with bigger μ and smaller α parameters.

Fig. 10 plots the OP of D_2 considering three system conditions: ideal condition ($\psi = 0; \varepsilon = 0$), the ImpSIC ($\psi = 0; \varepsilon = 0.1$) and the ImpSIC and RTHIs ($\psi = 0.1; \varepsilon = 0.1$). We can observe that for the ideal condition the system obtains the best outage performance. However, the system with the ImpSIC shows slightly worse performance in terms of the OP. This is due to the fact that imperfect detection of the message x_1 at D_2 decreases the level of SDIR for detecting its own message x_2 , which, subsequently, results in lower obtained outage performance. Then, when the ImpSIC and RTHIs are considered, it is noticed that the OP further degrades since HIs add additional interference level on the system. Finally, it is worth to mention that the RTHIs and ImpSIC have more impact on the OP at high SNR levels compared to lower ones.

V. CONCLUSION

In this paper, we analyzed the performance of the downlink DF-based underlay CR-NOMA relaying network over different α - μ fading channels such as Weibull, Nakagami- m and Rayleigh. We assumed three realistic factors namely ITC, ImpSIC and RTHIs to consider a practical network. Accurate closed-form analytical expressions for the end-to-end OP of two end-users were derived taking into account the primary interference. Moreover, we examined the impact of the fading parameters α and μ on the outage performance and found that the system performance can be sufficiently enhanced as α and/or μ are increased. Additionally, we derived several useful insights on the system performance by obtaining approximated closed-form OP expressions. Finally, the provided analytical closed-form expressions were verified by Monte Carlo simulations. In the future, this system model can

be extended by adding imperfect CSI for more practicality purpose. Moreover, some optimization problems, such as PA and the best relay selection among randomly located relays, will also be considered in the future work.

APPENDIXES

APPENDIX A

PROOF OF PROPOSITION 1

The term A in (18) can be rewritten as

$$A = \int_{z=0}^{\infty} f_Z(z) \int_{x=0}^{z\Delta_1} f_X(x) dx dz \int_{y=0}^R f_Y(y) dy. \quad (A.1)$$

The PDFs X, Y and Z abide by the $\alpha - \mu$ statistical model as shown in (1). Now, we modify these PDFs by applying the “change of variable” method [54]. Hence, the respective PDF can be rewritten as

$$f_{\xi}(r) = \frac{\alpha_{\xi} \lambda_{\xi}^{\mu_{\xi}} r^{\frac{\alpha_{\xi} \mu_{\xi}}{2} - 1}}{2\Gamma(\mu_{\xi})} \exp\left(-\lambda_{\xi} r^{\frac{\alpha_{\xi}}{2}}\right), \quad (A.2)$$

where $\xi = \{X, Y, Z\}$ and $\lambda_{\xi} = \mu_{\xi} / \hat{r}^{\frac{\alpha_{\xi}}{2}}$. Then, using (A.2), the term A can be further calculated as

$$A = \Omega_y \int_0^{\infty} \frac{\alpha_z \lambda_z z^{\frac{\alpha_z \mu_z}{2} - 1} e^{-\lambda_z z^{\frac{\alpha_z}{2}}}}{2\Gamma(\mu_z)} \times \frac{\gamma_{inc}\left(\mu_x, \lambda_x (z\Delta_1)^{\frac{\alpha_x}{2}}\right)}{\Gamma(\mu_x)} dz, \quad (A.3)$$

where $\Omega_y = \frac{\gamma_{inc}\left(\mu_y, \lambda_y \Delta_1^{\frac{\alpha_y}{2}}\right)}{\Gamma(\mu_y)}$. Now, by using the series representation of the lower incomplete Gamma function given by [59]

$$\gamma_{inc}(b, \xi) = \Gamma(b) - \Gamma(b) \exp(-\xi) \sum_{i=0}^{b-1} \frac{\xi^i}{i!}, \quad (A.4)$$

we can re-express the term A as

$$A = \Omega_y - \Omega_y \frac{\alpha_z \lambda_z^{\mu_z}}{2\Gamma(\mu_z)} \sum_{m=0}^{\mu_x - 1} \frac{\lambda_x^m \Delta_1^{\frac{\alpha_x m}{2}}}{m!} \times \underbrace{\int_0^{\infty} z^{\frac{\alpha_z \mu_z}{2} + \frac{\alpha_x m}{2} - 1} \exp\left(-\lambda_z z^{\frac{\alpha_z}{2}} - \lambda_x \Delta_1^{\frac{\alpha_x}{2}} z^{\frac{\alpha_x}{2}}\right) dz}_{A_1}. \quad (A.5)$$

To the best of our knowledge, the OP expression given by (A.5) cannot be solved in closed form without imposing certain assumptions.

Remark 2: It is important to note that the assumption of the same values of α does not limit our contribution, since this assumption of equal values is considered only for channel coefficients within one domain, while α parameter of the second domain may vary differently¹ i.e., $\alpha = \alpha_x = \alpha_y = \alpha_z$ and $\alpha_2 = \alpha_q = \alpha_v = \alpha_u = \alpha_w$, where given

¹For example, as shown in Fig. 1, α is considered for all solid lines in the first time slot, while α_2 is applied to all dashed lines in the second time slot.

indices correspond to the RVs. Simultaneously, parameters μ and λ can alter independently, which allow us to study not only the performance of the considered system with the same channel distributions, but also hybrid channels, i.e., Rayleigh / Weibull, Rayleigh / Nakagami- m , Weibull / Nakagami- m , Nakagami- m / Rayleigh, etc., for various values of m .

Keeping the assumption made in Remark 2 in mind, the term A_1 in (A.5) can be re-calculated as

$$A_1 = \int_0^\infty z^{\frac{\alpha}{2}(\mu_z+m)-1} e^{-z^{\frac{\alpha}{2}}(\lambda_z+\lambda_x\Delta_1^{\frac{\alpha}{2}})} dz = \frac{2\Gamma(\mu_z+m)}{\alpha(\lambda_z+\lambda_x\Delta_1^{\frac{\alpha}{2}})^{\mu_z+m}} \quad (A.6)$$

Now, inserting (A.6) into (A.5), we can write the term A in a closed-form as

$$A = \frac{\gamma_{inc}(\mu_y, \lambda_y\Lambda^{\frac{\alpha}{2}})}{\Gamma(\mu_y)} - \frac{\lambda_z^{\mu_z}\gamma_{inc}(\mu_y, \lambda_y\Lambda^{\frac{\alpha}{2}})}{\Gamma(\mu_y)\Gamma(\mu_z)} \times \sum_{m=0}^{\mu_x-1} \frac{\lambda_x^m\Delta_1^{\frac{\alpha m}{2}}\Gamma(\mu_z+m)}{m!(\lambda_z+\lambda_x\Delta_1^{\frac{\alpha}{2}})^{\mu_z+m}} \quad (A.7)$$

The second part of the CDF of $\gamma_{R,1}$, term B in (18), can be rewritten as follows

$$B = \int_{z=0}^\infty f_Z(z) \underbrace{\int_{y=R}^\infty \int_{x=0}^{yz\Delta_2} f_Y(y)f_X(x)dx dy}_{B_1} dz, \quad (A.8)$$

while the term B_1 in (A.8) can be calculated by

$$B_1 = \varepsilon \int_R^\infty y^{\frac{\alpha\mu_y}{2}-1} e^{-\lambda_y y^{\frac{\alpha}{2}}} dy - \varepsilon \Psi z^{\frac{\alpha m_2}{2}} \times \int_R^\infty y^{\frac{\alpha}{2}(\mu_y+m_2)-1} e^{-y^{\frac{\alpha}{2}}(\lambda_y+\lambda_x[z\Delta_2]^{\frac{\alpha}{2}})} dy = \frac{\Gamma(\mu_y, \lambda_y\Lambda^{\frac{\alpha}{2}})}{\Gamma(\mu_y)} - \frac{\Psi}{\Gamma(\mu_y)} \frac{\Gamma(\zeta, \Lambda^{\frac{\alpha}{2}}[\lambda_y+\lambda_x[z\Delta_2]^{\frac{\alpha}{2}}])}{[\lambda_y+\lambda_x[z\Delta_2]^{\frac{\alpha}{2}}]^\zeta}, \quad (A.9)$$

where $\zeta = \mu_y + m_2$, $\varepsilon = \frac{\alpha\lambda_y^{\mu_y}}{2\Gamma(\mu_y)}$ and $\Psi = \sum_{m_2=0}^{\mu_x-1} \frac{\lambda_x^{m_2}\Delta_2^{\frac{\alpha m_2}{2}}}{m_2!}$. Then, by inserting (A.9) into (A.8), and applying the series representation of the upper incomplete Gamma function of

$$\Gamma(b, c) = \Gamma(b) \exp(-c) \sum_{i=0}^{b-1} \frac{c^i}{i!} \quad (A.10)$$

and binomial series expansion [60], the term B can be further rewritten as

$$B = \frac{\Gamma(\mu_y, \lambda_y\Lambda^{\frac{\alpha}{2}})}{\Gamma(\mu_y)} - \frac{\alpha\lambda_y^{\mu_y}\lambda_z^{\mu_z}e^{-\lambda_y\Lambda^{\frac{\alpha}{2}}}\Psi\Gamma(\mu_y+m_2)}{2\Gamma(\mu_y)\Gamma(\mu_z)} \Theta \times \underbrace{\int_0^\infty \frac{z^{\frac{\alpha}{2}(\mu_z+m_2+s)-1} e^{-z^{\frac{\alpha}{2}}(\lambda_z+\lambda_x[R\Delta_2]^{\frac{\alpha}{2}})}}{\left(1+\frac{\lambda_x}{\lambda_y}[z\Delta_2]^{\frac{\alpha}{2}}\right)^\zeta} dz}_{B_2}, \quad (A.11)$$

where $\Theta = \sum_{i=0}^{\zeta-1} \frac{\lambda_y^i\Lambda^{\frac{\alpha i}{2}}}{i!} \sum_{s=0}^i \binom{i}{s} \frac{\lambda_x^s\Delta_2^{\frac{\alpha s}{2}}}{\lambda_y^{\mu_y+m_2+s}}$. By using the method of the *change of variable*, i.e., $t = z^{\frac{\alpha}{2}}$, and then representing $e^{-b\gamma}$ and $(1+c\gamma)^{-d}$ in terms of Meijer G-functions [61, Eqs. (7.34.3.46.1) and (7.34.3.271.1)] respectively as $G_{0,1}^{1,0} |_{-\ast} b\gamma$ and $\frac{1}{\Gamma(d)} G_{1,1}^{1,0} |_{1-d} \ast c\gamma$, and after some mathematical manipulations, the term B_2 in (A.11) can be written as

$$B_2 = \frac{2}{\alpha\Gamma(\zeta)} \int_0^\infty t^{\mu_z+m_2+s-1} G_{1,1}^{1,0} |_{1-\zeta} \ast \frac{\lambda_x}{\lambda_y} \Delta_2^{\frac{\alpha}{2}} t \times G_{0,1}^{1,0} \left(\left(\lambda_z + \lambda_x [R\Delta_2]^{\frac{\alpha}{2}} \right) t \middle| \frac{-}{0} \right) dt. \quad (A.12)$$

Now, utilizing [62, Eq. (21)] for B_2 , the term B in (18) can be written in closed-form as

$$B = \frac{\Gamma(\mu_y, \lambda_y\Lambda^{\frac{\alpha}{2}})}{\Gamma(\mu_y)} - \frac{\lambda_z^{\mu_z}\lambda_y^{\mu_z}e^{-\lambda_y\Lambda^{\frac{\alpha}{2}}}\Delta_2^{-\frac{\alpha\mu_z}{2}}}{\lambda_x^{\mu_z}\Gamma(\mu_y)\Gamma(\mu_z)} \times \sum_{m_2=0}^{\mu_x-1} \sum_{i=0}^{\zeta-1} \sum_{s=0}^i \binom{i}{s} \frac{\lambda_y^i\Lambda^{\frac{\alpha i}{2}}}{m_2!i!} G_{1,2}^{2,1} \times \left(\frac{\left(\lambda_z + \lambda_x [\Lambda\Delta_2]^{\frac{\alpha}{2}} \right)}{\lambda_y^{-1}\lambda_x\Delta_2^{\frac{\alpha}{2}}} \middle| \begin{matrix} 0, -\mu_z + \mu_y - s \\ 1 - (\mu_z + m_2 + s) \end{matrix} \right). \quad (A.13)$$

Finally, by inserting (A.7) and (A.13) into (18), the CDF of $\gamma_{R,1}$ can be written in its closed-form as in (19), where $\theta_1 < \frac{\rho_1}{\rho_2 + \varphi_{SR}^2}$, otherwise, $F_{\gamma_{R,1}}(\theta_1) \sim 1$. ■

APPENDIX B DERIVATION OF HIGH SNR APPROXIMATED OUTAGE PROBABILITY

Considering the asymptotic ITC in (26), the CDF of $\gamma_{R,1}$ for a high SNR can be written as

$$F_{\gamma_{R,1}}^{HS} = \Pr[X < YZ\Delta_2] = \int_{z=0}^\infty f_Z(z) \underbrace{\int_{y=0}^\infty \int_{x=0}^{yz\Delta_2} f_Y(y)f_X(x)dx dy}_{B^*} dz. \quad (B.1)$$

Considering high SNR approximations for the lower and upper incomplete gamma functions as $\gamma_{inc}(c, d) \approx \frac{d^c}{c}$ and $\Gamma(c, d) \approx \Gamma(c)$, $d \rightarrow 0$ [33], we can rewrite B^* as follows

$$B^* = \frac{\alpha\lambda_x^{\mu_x}\lambda_y^{\mu_y}\Delta_2^{\frac{\alpha\mu_x}{2}}z^{\frac{\alpha\mu_x}{2}}}{2\mu_x\Gamma(\mu_x)\Gamma(\mu_y)} \int_0^\infty y^{\frac{\alpha}{2}(\mu_x+\mu_y)-1} e^{-\lambda_y y^{\frac{\alpha}{2}}} dy = \frac{\lambda_x^{\mu_x}\Delta_2^{\frac{\alpha\mu_x}{2}}z^{\frac{\alpha\mu_x}{2}}\Gamma(\mu_x+\mu_y)}{\lambda_y^{\mu_x}\mu_x\Gamma(\mu_x)\Gamma(\mu_y)}. \quad (B.2)$$

Then, after inserting (B.2) into (B.1) and some mathematical manipulations, the CDF of $\gamma_{R,1}$ for a high SNR can be written in the closed-form as

$$F_{\gamma_{R,1}}^{HS} = \frac{\lambda_x^{\mu_x}\Delta_2^{\frac{\alpha\mu_x}{2}}\Gamma(\mu_x+\mu_y)\Gamma(\mu_x+\mu_z)}{\lambda_y^{\mu_x}\lambda_z^{\mu_z}\mu_x\Gamma(\mu_x)\Gamma(\mu_y)\Gamma(\mu_z)}. \quad (B.3)$$

Further, the CDFs of $\gamma_{R,2}$, γ_1 and γ_2 for the high SNR approximation can be calculated following the same steps as in (B.1)-(B.3). Finally, the high SNR approximated OP of D_1 and D_2 can be respectively found by using (17) and (22) and written as in (27) and (28), accordingly. ■

**APPENDIX C
DERIVATION OF OUTAGE PROBABILITY FOR NO ITC
IMPOSED MODEL**

Considering no transmit power restriction at secondary transmit nodes, i.e., $L_{ITC} \rightarrow \infty$, we can rewrite (19) as follows

$$\begin{aligned}
 F_{\gamma_{R,1}}^\infty(\theta_1) &= \Pr \left[\frac{\rho_1 T_S |g_{SR}|^2}{\rho_2 T_S |g_{SR}|^2 + T_P |g_{PR}|^2} < \theta_1 \right] \\
 &= \Pr [X < Z \Delta_1] = \int_{z=0}^\infty f_Z(z) \int_{x=0}^{z \Delta_1} f_X(x) dx dz \\
 &= \int_0^\infty \frac{\alpha_z \lambda_z^{\mu_z} z^{\frac{\alpha \mu_z}{2} - 1} e^{-\lambda_z z^{\frac{\alpha}{2}}}}{2\Gamma(\mu_z)} \frac{\gamma_{inc} \left(\mu_x, \lambda_x (z \Delta_1)^{\frac{\alpha}{2}} \right)}{\Gamma(\mu_x)} dz.
 \end{aligned} \tag{C.1}$$

Furthermore, applying the series representation of the lower incomplete Gamma function as in (A.4) and after some mathematical manipulations, (C.1) can be written in a closed-form as

$$F_{\gamma_{R,1}}^\infty(\theta_1) = 1 - \frac{1}{\Gamma(\mu_z)} \sum_{m=0}^{\mu_x - 1} \frac{\Gamma(\mu_z + m) \lambda_x^m \Delta_1^{\frac{\alpha m}{2}}}{m! \left(\lambda_z + \lambda_x \Delta_1^{\frac{\alpha}{2}} \right)^{\mu_z + m}}. \tag{C.2}$$

Now, following the similar approach as in (C.1) and (C.2), the CDF of γ_1 for the considered model can be written in its closed-form as

$$F_{\gamma_1}^\infty(\theta_1) = 1 - \frac{1}{\Gamma(\mu_w)} \sum_{k=0}^{\mu_q - 1} \frac{\Gamma(\mu_w + k) \lambda_q^k \Phi_1^{\frac{\alpha_2 k}{2}}}{k! \left(\lambda_w + \lambda_q \Phi_1^{\frac{\alpha_2}{2}} \right)^{\mu_w + k}}. \tag{C.3}$$

Finally, the OP of D_1 for the proposed asymptotic model can be derived after inserting (C.2) and (C.3) into (17). The OP for D_2 can be found similarly.

ACKNOWLEDGMENT

The authors would like to acknowledge Dr. Abdulkadir Celik for useful discussions.

REFERENCES

[1] Z. Kuang, G. Liu, G. Li, and X. Deng, "Energy efficient resource allocation algorithm in energy harvesting-based D2D heterogeneous networks," *IEEE Internet Things J.*, vol. 6, no. 1, pp. 557–567, Feb. 2019.
 [2] S. J. Ambroziak, L. M. Correia, R. J. Katulski, M. Mackowiak, C. Oliveira, J. Sadowski, and K. Turbic, "An off-body channel model for body area networks in indoor environments," *IEEE Trans. Antennas Propag.*, vol. 64, no. 9, pp. 4022–4035, Sep. 2016.
 [3] S. Kumar, U. Dohare, K. Kumar, D. Prasad Dora, K. N. Qureshi, and R. Kharel, "Cybersecurity measures for geocasting in vehicular cyber physical system environments," *IEEE Internet Things J.*, vol. 6, no. 4, pp. 5916–5926, Aug. 2019.

[4] A. Celik, R. M. Radaydeh, F. S. Al-Qahtani, and M.-S. Alouini, "Resource allocation and interference management for D2D-enabled DL/UL decoupled het-nets," *IEEE Access*, vol. 5, pp. 22735–22749, 2017.
 [5] J. H. Anajemba, Y. Tang, J. A. Ansere, and C. Iwendi, "Performance analysis of D2D energy efficient IoT networks with relay-assisted underlying technique," in *Proc. 44th Annu. Conf. IEEE Ind. Electron. Soc. (IECON)*, Oct. 2018, pp. 3864–3869.
 [6] J. Reed, M. Vassiliou, and S. Shah, "The role of new technologies in solving the spectrum shortage [point of view]," *Proc. IEEE*, vol. 104, no. 6, pp. 1163–1168, Jun. 2016.
 [7] Z. Ding, X. Lei, G. K. Karagiannidis, R. Schober, J. Yuan, and V. K. Bhargava, "A survey on non-orthogonal multiple access for 5G networks: Research challenges and future trends," *IEEE J. Sel. Areas Commun.*, vol. 35, no. 10, pp. 2181–2195, Oct. 2017.
 [8] Z. Ding, Y. Liu, J. Choi, Q. Sun, M. Elkashlan, C.-L. I, and H. V. Poor, "Application of non-orthogonal multiple access in LTE and 5G networks," *IEEE Commun. Mag.*, vol. 55, no. 2, pp. 185–191, Feb. 2017.
 [9] Y. Cai, Z. Qin, F. Cui, G. Y. Li, and J. A. McCann, "Modulation and multiple access for 5G networks," *IEEE Commun. Surveys Tuts.*, vol. 20, no. 1, pp. 629–646, 1st Quart., 2018.
 [10] Z. Yang, Z. Ding, P. Fan, and G. K. Karagiannidis, "On the performance of non-orthogonal multiple access systems with partial channel information," *IEEE Trans. Commun.*, vol. 64, no. 2, pp. 654–667, Feb. 2016.
 [11] A. Al-Fuqaha, M. Guizani, M. Mohammadi, M. Aledhari, and M. Ayyash, "Internet of Things: A survey on enabling technologies, protocols, and applications," *IEEE Commun. Surveys Tuts.*, vol. 17, no. 4, pp. 2347–2376, 4th Quart., 2015.
 [12] D. S. Gurjar, H. H. Nguyen, and H. D. Tuan, "Wireless information and power transfer for IoT applications in overlay cognitive radio networks," *IEEE Internet Things J.*, vol. 6, no. 2, pp. 3257–3270, Apr. 2019.
 [13] Y. Gao, B. Xia, K. Xiao, Z. Chen, X. Li, and S. Zhang, "Theoretical analysis of the dynamic decode ordering SIC receiver for uplink NOMA systems," *IEEE Commun. Lett.*, vol. 21, no. 10, pp. 2246–2249, Oct. 2017.
 [14] B. Xia, J. Wang, K. Xiao, Y. Gao, Y. Yao, and S. Ma, "Outage performance analysis for the advanced SIC receiver in wireless NOMA systems," *IEEE Trans. Veh. Technol.*, vol. 67, no. 7, pp. 6711–6715, Jul. 2018.
 [15] Z. Ding, Z. Yang, P. Fan, and H. V. Poor, "On the performance of non-orthogonal multiple access in 5G systems with randomly deployed users," *IEEE Signal Process. Lett.*, vol. 21, no. 12, pp. 1501–1505, Dec. 2014.
 [16] X. Wang, J. Wang, L. He, and J. Song, "Outage analysis for downlink NOMA with statistical channel state information," *IEEE Wireless Commun. Lett.*, vol. 7, no. 2, pp. 142–145, Apr. 2018.
 [17] A. Celik, M.-C. Tsai, R. M. Radaydeh, F. S. Al-Qahtani, and M.-S. Alouini, "Distributed cluster formation and power-bandwidth allocation for imperfect NOMA in DL-HetNets," *IEEE Trans. Commun.*, vol. 67, no. 2, pp. 1677–1692, Feb. 2019.
 [18] A. Celik, M.-C. Tsai, R. M. Radaydeh, F. S. Al-Qahtani, and M.-S. Alouini, "Distributed user clustering and resource allocation for imperfect NOMA in heterogeneous networks," *IEEE Trans. Commun.*, vol. 67, no. 10, pp. 7211–7227, Oct. 2019.
 [19] Z. Xiang, W. Yang, G. Pan, Y. Cai, Y. Song, and Y. Zou, "Secure transmission in HARQ-assisted non-orthogonal multiple access networks," *IEEE Trans. Inf. Forensics Security*, vol. 15, pp. 2171–2182, 2020.
 [20] Z. Xiang, W. Yang, Y. Cai, Z. Ding, and Y. Song, "Secure transmission design in HARQ assisted cognitive NOMA networks," *IEEE Trans. Inf. Forensics Security*, vol. 15, pp. 2528–2541, 2020.
 [21] L. Zhang, J. Liu, M. Xiao, G. Wu, Y.-C. Liang, and S. Li, "Performance analysis and optimization in downlink NOMA systems with cooperative full-duplex relaying," *IEEE J. Sel. Areas Commun.*, vol. 35, no. 10, pp. 2398–2412, Oct. 2017.
 [22] N. Guo, J. Ge, C. Zhang, Q. Bu, and P. Tian, "Non-orthogonal multiple access in full-duplex relaying system with Nakagami-*m* fading," *IET Commun.*, vol. 13, no. 3, pp. 271–280, Feb. 2019.
 [23] Y. Li, Y. Li, X. Chu, Y. Ye, and H. Zhang, "Performance analysis of relay selection in cooperative NOMA networks," *IEEE Commun. Lett.*, vol. 23, no. 4, pp. 760–763, Apr. 2019.
 [24] A. Sendonaris, E. Erkip, and B. Aazhang, "User cooperation diversity—Part I: System description," *IEEE Trans. Commun.*, vol. 51, no. 11, pp. 1927–1938, Nov. 2003.
 [25] J. N. Laneman, D. N. C. Tse, and G. W. Wornell, "Cooperative diversity in wireless networks: Efficient protocols and outage behavior," *IEEE Trans. Inf. Theory*, vol. 50, no. 12, pp. 3062–3080, Dec. 2004.

- [26] Z. Ding, M. Peng, and H. V. Poor, "Cooperative non-orthogonal multiple access in 5G systems," *IEEE Commun. Lett.*, vol. 19, no. 8, pp. 1462–1465, Aug. 2015.
- [27] J.-B. Kim and I.-H. Lee, "Non-orthogonal multiple access in coordinated direct and relay transmission," *IEEE Commun. Lett.*, vol. 19, no. 11, pp. 2037–2040, Nov. 2015.
- [28] C. Zhong and Z. Zhang, "Non-orthogonal multiple access with cooperative full-duplex relaying," *IEEE Commun. Lett.*, vol. 20, no. 12, pp. 2478–2481, Dec. 2016.
- [29] J. Men, J. Ge, and C. Zhang, "Performance analysis of nonorthogonal multiple access for relaying networks over Nakagami- m fading channels," *IEEE Trans. Veh. Technol.*, vol. 66, no. 2, pp. 1200–1208, Feb. 2017.
- [30] Z. Yang, Z. Ding, Y. Wu, and P. Fan, "Novel relay selection strategies for cooperative NOMA," *IEEE Trans. Veh. Technol.*, vol. 66, no. 11, pp. 10114–10123, Nov. 2017.
- [31] P. Xu, Z. Yang, Z. Ding, and Z. Zhang, "Optimal relay selection schemes for cooperative NOMA," *IEEE Trans. Veh. Technol.*, vol. 67, no. 8, pp. 7851–7855, Aug. 2018.
- [32] L. Lv, J. Chen, Q. Ni, and Z. Ding, "Design of cooperative non-orthogonal multicast cognitive multiple access for 5G systems: User scheduling and performance analysis," *IEEE Trans. Commun.*, vol. 65, no. 6, pp. 2641–2656, Jun. 2017.
- [33] C. Zhong, T. Ratnarajah, and K.-K. Wong, "Outage analysis of decode-and-forward cognitive dual-hop systems with the interference constraint in Nakagami- m fading channels," *IEEE Trans. Veh. Technol.*, vol. 60, no. 6, pp. 2875–2879, Jul. 2011.
- [34] N. I. Miridakis, S. Arzykulov, T. A. Tsiftsis, G. Yang, and G. Nauryzbayev, "Green CR-NOMA: A new interweave energy harvesting transmission scheme for secondary access," in *Proc. 16th Int. Symp. Wireless Commun. Syst. (ISWCS)*, Aug. 2019, pp. 571–576.
- [35] G. Nauryzbayev, S. Arzykulov, T. A. Tsiftsis, and M. Abdallah, "Performance of cooperative underlay CR-NOMA networks over Nakagami- m channels," in *Proc. IEEE Int. Conf. Commun. Workshops (ICC Workshops)*, May 2018, pp. 1–6.
- [36] A. Goldsmith, S. A. Jafar, I. Maric, and S. Srinivasa, "Breaking spectrum gridlock with cognitive radios: An information theoretic perspective," *Proc. IEEE*, vol. 97, no. 5, pp. 894–914, May 2009.
- [37] M. Liu, L. Liu, H. Song, Y. Hu, Y. Yi, and F. Gong, "Signal estimation in underlay cognitive networks for industrial Internet of Things," *IEEE Trans. Ind. Informat.*, early access, Nov. 8, 2019, doi: [10.1109/TII.2019.2952413](https://doi.org/10.1109/TII.2019.2952413).
- [38] F. Khan, A. U. Rehman, M. A. Jan, and I. U. Rahman, "Efficient resource allocation for real time traffic in cognitive radio Internet of Things," in *Proc. Int. Conf. Internet Things (iThings) IEEE Green Comput. Commun. (GreenCom) IEEE Cyber, Phys. Social Comput. (CPSCom) IEEE Smart Data (SmartData)*, Jul. 2019, pp. 1143–1147.
- [39] Y. Liu, Z. Ding, M. ElKashlan, and J. Yuan, "Nonorthogonal multiple access in large-scale underlay cognitive radio networks," *IEEE Trans. Veh. Technol.*, vol. 65, no. 12, pp. 10152–10157, Dec. 2016.
- [40] L. Lv, Q. Ni, Z. Ding, and J. Chen, "Application of non-orthogonal multiple access in cooperative spectrum-sharing networks over Nakagami- m fading channels," *IEEE Trans. Veh. Technol.*, vol. 66, no. 6, pp. 5506–5511, Jun. 2017.
- [41] Y. Chen, L. Wang, and B. Jiao, "Cooperative multicast non-orthogonal multiple access in cognitive radio," in *Proc. IEEE Int. Conf. Commun. (ICC)*, May 2017, pp. 1–6.
- [42] J. Si, Z. Li, X. Chen, B. Hao, and Z. Liu, "On the performance of cognitive relay networks under primary user's outage constraint," *IEEE Commun. Lett.*, vol. 15, no. 4, pp. 422–424, Apr. 2011.
- [43] S. Arzykulov, G. Nauryzbayev, T. A. Tsiftsis, and B. Maham, "Performance analysis of underlay cognitive radio nonorthogonal multiple access networks," *IEEE Trans. Veh. Technol.*, vol. 68, no. 9, pp. 9318–9322, Sep. 2019.
- [44] S. Kim, W. Choi, Y. Choi, J. Lee, Y. Han, and I. Lee, "Downlink performance analysis of cognitive radio based cellular relay networks," in *Proc. 3rd Int. Conf. Cognit. Radio Oriented Wireless Netw. Commun. (CrownCom)*, May 2008, pp. 1–6.
- [45] L. Tlebaldiyeva, B. Maham, and T. A. Tsiftsis, "Device-to-device mmWave communication in the presence of interference and hardware distortion noises," *IEEE Commun. Lett.*, vol. 23, no. 9, pp. 1607–1610, Sep. 2019.
- [46] E. Bjornson, J. Hoydis, M. Kountouris, and M. Debbah, "Massive MIMO systems with non-ideal hardware: Energy efficiency, estimation, and capacity limits," *IEEE Trans. Inf. Theory*, vol. 60, no. 11, pp. 7112–7139, Nov. 2014.
- [47] E. Bjornson, P. Zetterberg, M. Bengtsson, and B. Ottersten, "Capacity limits and multiplexing gains of MIMO channels with transceiver impairments," *IEEE Commun. Lett.*, vol. 17, no. 1, pp. 91–94, Jan. 2013.
- [48] B. Selim, S. Muhaidat, P. C. Sofotasios, A. Al-Dweik, B. S. Sharif, and T. Stouraitis, "Radio-frequency front-end impairments: Performance degradation in nonorthogonal multiple access communication systems," *IEEE Veh. Technol. Mag.*, vol. 14, no. 1, pp. 89–97, Mar. 2019.
- [49] D. K. Nguyen and H. Ochi, "Transceiver impairments in DF/AF dual-hop cognitive relay networks: Outage performance and throughput analysis," in *Proc. IEEE 81st Veh. Technol. Conf. (VTC Spring)*, May 2015, pp. 1–5.
- [50] L. Tlebaldiyeva and T. Tsiftsis, "Underlay cognitive radio with imperfect transceiver electronics under Nakagami- m fading," in *Proc. Int. Conf. Comput. Netw. Commun. (CoCoNet)*, Aug. 2018, pp. 58–63.
- [51] X. Li, J. Li, Y. Liu, Z. Ding, and A. Nallanathan, "Residual transceiver hardware impairments on cooperative NOMA networks," *IEEE Trans. Wireless Commun.*, vol. 19, no. 1, pp. 680–695, Jan. 2020.
- [52] I. S. Gradshteyn and I. M. Ryzhik, *Table of Integrals, Series, and Products*, 7th ed. Amsterdam, The Netherlands: Elsevier, 2007.
- [53] M. D. Yacoub, "The α - μ distribution: A physical fading model for the Stacy distribution," *IEEE Trans. Veh. Technol.*, vol. 56, no. 1, pp. 27–34, Jan. 2007.
- [54] G. Nauryzbayev, K. M. Rabie, M. Abdallah, and B. Adebisi, "On the performance analysis of WPT-based dual-hop AF relaying networks in α - μ fading," *IEEE Access*, vol. 6, pp. 37138–37149, 2018.
- [55] S. Arzykulov, G. Nauryzbayev, T. A. Tsiftsis, B. Maham, and M. Abdallah, "On the outage of underlay CR-NOMA networks with Detect-and-Forward relaying," *IEEE Trans. Cognit. Commun. Netw.*, vol. 5, no. 3, pp. 795–804, Sep. 2019.
- [56] O. L. Alcaraz Lopez, H. Alves, P. H. Juliano Nardelli, and M. Latva-Aho, "Aggregation and resource scheduling in machine-type communication networks: A stochastic geometry approach," *IEEE Trans. Wireless Commun.*, vol. 17, no. 7, pp. 4750–4765, Jul. 2018.
- [57] S. Niknam and B. Natarajan, "On the regimes in millimeter wave networks: Noise-limited or interference-limited?" in *Proc. IEEE Int. Conf. Commun. Workshops (ICC Workshops)*, May 2018, pp. 1–6.
- [58] A. Goldsmith, *Wireless Communications*. Cambridge, U.K.: Cambridge Univ. Press, 2005.
- [59] S. Arzykulov, G. Nauryzbayev, and T. A. Tsiftsis, "Underlay cognitive relaying system over α - μ fading channels," *IEEE Commun. Lett.*, vol. 21, no. 1, pp. 216–219, Jan. 2017.
- [60] G. B. Arfken, *Mathematical Methods for Physicists*, 3rd ed. San Diego, CA, USA: Academic, 1985.
- [61] Wolfram. (Apr. 11, 2020). *The Wolfram Functions Site*. [Online]. Available: <http://functions.wolfram.com>
- [62] V. S. Adamchik and O. I. Marichev, "The algorithm for calculating integrals of hypergeometric type functions and its realization in REDUCE system," in *Proc. Int. Symp. Symbolic Algebr. Comput. (ISSAC)*, New York, NY, USA, 1990, pp. 212–224.



SULTANGALI ARZYKULOV (Member, IEEE)

received the B.Sc. degree (Hons.) in radio engineering, electronics and telecommunications from Kazakh National Research Technical University after K. I. Satpayev, Almaty, Kazakhstan, in June 2010, the M.Sc. degree in communication engineering from The University of Manchester, Manchester, U.K., in 2013, and the Ph.D. degree in science, engineering and technology from Nazarbayev University, Nur-Sultan, Kazakhstan, in 2019. He is currently a Postdoctoral Scholar with Nazarbayev University, Kazakhstan. His research interests include broad areas of wireless communication systems, with particular focus on cooperative communications, cognitive radio, energy harvesting, interference mitigation, and NOMA. He acts as a Reviewer for several international journals/conferences and served as a technical program committee member of numerous IEEE Communication Society flagship conferences.



GALYMZHAN NAURYZBAYEV (Member, IEEE) received the B.Sc. and M.Sc. (Hons.) degrees in radio engineering, electronics, and telecommunications from the Almaty University of Power Engineering and Telecommunication, Almaty, Kazakhstan, in 2009 and 2011, respectively, and the Ph.D. degree in wireless communications from The University of Manchester, U.K., in 2016. From 2016 to 2018, he held several academic and research positions with Nazarbayev University, Kazakhstan, L.N. Gumilyov Eurasian National University, Kazakhstan, and Hamad Bin Khalifa University, Qatar. In 2019, he joined Nazarbayev University, as an Assistant Professor. His research interest is in the area of wireless communication systems, with particular focus on multiuser MIMO systems, cognitive radio, signal processing, energy harvesting, visible light communications, NOMA, and interference mitigation. He served as a technical program committee member of numerous IEEE flagship conferences.



MOHAMMAD S. HASHMI (Senior Member, IEEE) received the B.Tech. degree from Aligarh Muslim University, India, the M.S. degree from the Darmstadt University of Technology, Germany, and the Ph.D. degree from Cardiff University, Cardiff, U.K. He had held research and engineering positions with the University of Calgary, Canada, Cardiff University, U.K.; Thales Electronics GmbH, Germany, and Philips Technology Center, Germany. He is currently an Associate

Professor at Nazarbayev University, Kazakhstan, and also holds a faculty position at IIT Delhi, India. His current research interests are in advanced RF circuits, broadband linear and efficient power amplifiers for mobile and satellite applications, and high and low-frequency instrumentation. His research activities have led to one book and over 180 journal and conference publications and holds three U.S. patents (two pending). He is an Associate Editor of the *IEEE Microwave Magazine*.



AHMED M. ELTAWIL (Senior Member, IEEE) received the Ph.D. degree from the University of California at Los Angeles, in 2003, and the B.Sc. and M.Sc. degrees (Hons.) from Cairo University, Giza, Egypt, in 1997 and 1999, respectively. Since 2019, he has been a Professor with the Computer, Electrical and Mathematical Science and Engineering Division (CEMSE), King Abdullah University of Science and Technology (KAUST), Thuwal, Saudi Arabia. Since 2005, he has been

with the Department of Electrical Engineering and Computer Science, University of California at Irvine, where he was the Founder and the Director of the Wireless Systems and Circuits Laboratory. His research interests are in the general area of low power digital circuit and signal processing architectures with an emphasis on mobile systems. He received several awards, as well as distinguished grants, including the NSF CAREER Grant, supporting his research in low power systems. He has been on the technical program committees and steering committees for numerous workshops, symposia, and conferences in the areas of low power computing and wireless communication system design.



KHALED M. RABIE (Member, IEEE) received the M.Sc. and Ph.D. degrees in electrical and electronic engineering from The University of Manchester, in 2011 and 2015, respectively. He is currently an Assistant Professor with the Department of Engineering, Manchester Metropolitan University (MMU), U.K. He has worked as a part of several largescale industrial projects and has published more than 100 journal and conference papers (mostly in IEEE). His primary research

focuses on various aspects of the next-generation wireless communication systems. He is also a Fellow of the U.K. Higher Education Academy (FHEA). He serves regularly on the Technical Program Committee (TPC) of several major IEEE conferences, such as GLOBECOM, ICC, and VTC. He has received numerous awards over the past few years in recognition of his research contributions, including the Best Student Paper Award at the IEEE ISPLC, TX, USA, in 2015, the MMU Outstanding Knowledge Exchange Project Award of 2016, as well as IEEE ACCESS Editor of the Month Award for August 2019. He serves as an Editor of the IEEE COMMUNICATIONS LETTERS, an Associate Editor of IEEE ACCESS, an Area Editor of *Physical Communications*, Elsevier, and an Executive Editor of the *Transactions on Emerging Telecommunications Technologies*.



SHAKHMARAN SEILOV received the Candidate degree in technical sciences from the Moscow Technical University of Communications and Informatics, Moscow, Russia, in 1989, and the Specialist degree from the Bonch-Bruевич Saint-Petersburg State University of Telecommunications, Saint-Petersburg, Russia, in 1983. He had held several positions, e.g., an Advisor of the First Deputy of the Prime Minister of the Republic of Kazakhstan and the President of NJSC Kazakhtelecom.

From 2015 to February 2019, he worked as the Head of the Department of Radio Engineering, Electronics and Telecommunications, L.N. Gumilyov Eurasian National University (ENU), Nur-Sultan, Kazakhstan. He is currently the Dean of the Information Technologies Faculty, ENU. He published more than 70 scientific articles and three monographs on the problems of state regulation of telecommunications and development and implementation of digital broadcasting.

...